Path Integral Quantum Monte Carlo Simulations of Atomic Rings

Stephan Richter

Supervisor: Ian Galbraith
Moderator: Weiping Lu

March 20, 2009

Abstract

In this project a numerical approach to the description of indistinguishable, interacting, ultra cold bosons on a ring in terms of Path Integral Monte Carlo (PIQMC) was realised. The code, based on a previous project dealing with electrons, was verified with analytical results (where possible) as well as results obtained from other numerical solutions and showed very good consistency. Different kinds of interactions were implemented, most importantly a dipole-dipole interaction. The ground state configuration for this system was discovered. Furthermore an attempt was done to force the system to show frustration behaviour, usually known from systems including antiferromagnetically coupling. We were able to show that frustration can be realised in such a system, although an experimental realisation would be, if possible at all, quite challenging. Finally the behaviour of the frustration signature compared to temperature and the number of particles was observed. PIQMC turned out to be well suited for a many body system with arbitrary interactions in the used ultra low temperature regime.

Contents

1 Introduction

In this project the properties of a many body quantum system in form of an atomic ring was investigated. This was done numerically by using the path integral quantum Monte Carlo method (PIQMC). The potentials that were implemented are an external potential along the ring as well as pair interactions, namely a Lennard Jones like repulsive and an attractive dipole potential.

1.1 Atomic rings

An atomic ring is a one dimensional (or quasi one dimensional) system with periodic boundary conditions. In our approach we used an exact one dimensional system, what can be realised experimentally by making the ring confinement sufficiently high to only allow the first (transverse) quantum state to be occupied at the temperatures used.

For many years such systems were used for theoretical modelling, since the one dimensionality and the periodic boundary conditions, and therefore no finite size effects, make it easy to handle. Recently it became possible to realise such systems experimentally for ultra cold atoms. This was achieved by an optical lattice which, in its easiest form, is created by counterpropagating beams of laser light. These beams are made to interfer creating a standing wave and therefore a spatially constant, oscillating periodic intensity field. If the oscillation is sufficiently high, the atoms can still be kept confined. The actual force keeping the atoms in place, is due to the Stark shift, describing the dependency of the atomic states from an external electric field. The form of the lattice can for example be manipulated using spatial light modulators that are used as configurable diffractive components. [8]

Given these new possibilities, results at finite temperatures for such systems become important for what the PIQMC is perfectly suited.

1.2 Tonks-Girardeau gas

One of the most interesting ultra cold quantum systems is the so called *Tonks-Girardeau gas*, proposed already 40 years ago [10]. It is a gas of Bose particles, confined in one dimension, in which the repulsion between the bosons dominate the behaviour of the system. The motion of two next neighbours are strongly correlated and two particles cannot be at the same position simultaneously. Therefore this repulsions mimics, although one deals with bosons, the Pauli principle. However, the statistics of such a gas is neither fermionic nor bosonic, since the particles in such a gas can all occupy the same momentum state which fermions cannot. Though mathematically there is a theorem mapping such strong repulsive bosons on non interacting

fermions [10]. It is described as an isomorphism, i.e. a mapping that is homomorph in both directions and therefore structure-preserving [10].

For long time there was no experimental realization of such a system until in 2004 an experiment realising a Tonks-Girardeau gas was presented [12]. The basic setup was a very strong two dimensional lattice, forcing the atoms into tubes and prohibiting tunnelling between them. By applying a third lattice potential in the remaining direction and increasing it, the effective mass was changed and thus the interactions became more important (tunnelling in the third direction was still allowed). As the interacting energy overcame the tunnel energy, tunnelling into occupied lattice points became suppressed, what produced the Tonks-Girardeau regime.

1.3 Dipolar gases

Another system, in a sense an extension to the above mentioned Tonks-Girardeau gas, sometimes called the Super-Tonks-Girardeau regime, is a one dimensional dipolar gas. Very recently such systems were under investigation in both, quasi one dimensional [3] and exact one dimensional traps in [1] and [2]. All of them included a repulsive potential independent of the alignment, i.e. not introducing additional dimensions for the dipole orientation, whereas in this project the exact dipole-dipole interaction was implemented taking the orientation of every dipole into account.

1.4 Frustrated systems

The term *frustration* was introduced by Gerard Toulouse in 1977 in his work on spin glasses [14]. Summarising, frustration is either caused by the fact, that a system cannot minimise competing interactions or by a lattice or configuration that does not allow the components, e.g. spins, to align in a unique way minimising the energy. The first observation of frustration was due to Wanier in 1950 [15]. He investigated antiferromagnetically coupled Ising spins on a triangular lattice and found its behaviour differing from a ferromagnetic coupled system. More precisely he found the binding energy to be much smaller as well as the entropy not vanishing for zero temperature.

1.5 The path integral quantum Monte Carlo method

The first applications of path integral theory, developed by Feynman in 1948 [5], were analytical calculations in quantum electro dynamics [6] and the theory of liquid helium [7]. Consequently, with increasing computer power, path integrals for liquid helium systems were calculated making use of Monte Carlo Methods [4]. Today PIQMC is employed in a wide range of fields.

The main advantages are the possibility to include arbitrary potentials and simulate in a wide temperature range, i.e. not only obtain the ground state energy but also thermodynamic averages of properties in systems at finite temperatures. Furthermore the method is, in principle, independent of the geometry of the system to be observed and proceeds without putting in any specific physical knowledge like trial wavefunctions. Difficulties are the large amount of parameters possibly influencing the result whose influence has to be observed as well as the long computing times that are necessary to reduce the statistical error sufficiently.

1.6 Report layout

Apart from this introduction this report is structured into four main sections. In the first one I will review the theoretical basis of the PIQMC method. The description of a system in terms of path integrals will be derived and the principles of Monte Carlo and Metropolis simulations are presented. In the second part the actual implementation of the PIQMC algorithm is described. The handling of physical features like symmetrisation and calculation of the total energy are specified. The following part consits of the obtained results for the above mentioned systems. These are basically particle distributions, correlation functions as well as temperature dependences of physical quantities. Finally in the conclusion I will summarise the results, point out the essentials as well as problems. Following on from this recommendations for further research will be made.

2 Theory

In order to understand how the PIQMC algorithm works one needs some theoretical knowledge about the fundamental physics employed in these simulations. This is mainly the Path Integral Theory introduced by Feynman in 1948 [5]. Furthermore one needs the so called Monte Carlo Approach allowing us to sample through the infinite number of possible paths that are given by Feynman's formulation.

2.1 Path integral theory

In his work Feynman describes a new formulation of quantum mechanics based on paths through configuration space and closely connected to Lagrange's formulation of classical mechanics. In this formulation *Lagrange's equations*, determining the actual realized path of a system in time through the configuration space from A to B, are derived by minimising the action of the system in question.

$$S = \int_A^B \mathcal{L}(\vec{x}, \dot{\vec{x}}, t)\mathrm{d}t \tag{1}$$

Here $\mathcal{L}$ is the Lagrangian of the system and $\vec{x}$ is the dN-dimensional vector in configuration space, $\dot{\vec{x}}$ the corresponding velocity. Why nature behaves as this process tells us, no one really

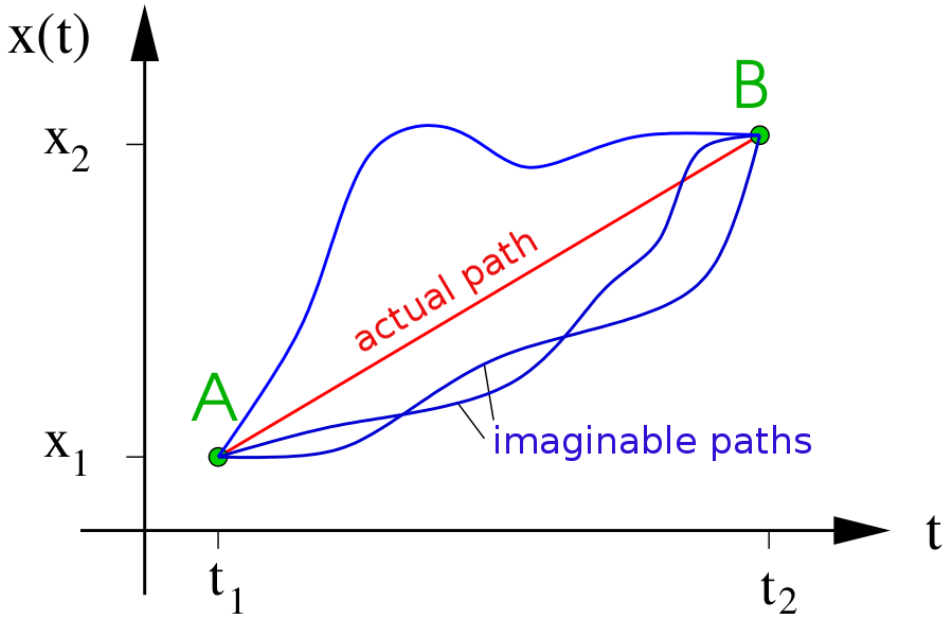

Figure 1: paths from A to B

knows.

Feynman's approach answers this question by saying, that actually all imaginable paths are realised, but we only "see" the interference of all these possibilities. More precisely one can express the wavefunction at (x,t) (given a start point (x_0,t_0) with amplitude 1) as

$$\Psi(x,t) \propto \sum_{C_{(x_0,t_0)\to(x,t)}} \mathrm{e}^{\frac{i}{\hbar}S[C]} \tag{2}$$

This implies that the probability to find a particle at position x at time t after it started at (x_0,t_0), known as the propagator K is

$$K(x,t,x_0,t_0) = \langle x|\mathrm{e}^{-\frac{i}{\hbar}\mathcal{H}\cdot(t-t_0)}|x_0\rangle \propto \sum_{C_{(x_0,t_0)\to(x,t)}} \mathrm{e}^{\frac{i}{\hbar}S[C]} \tag{3}$$

(the definition of the propagator is only valid for time independent Hamiltonians).

2.1.1 Derivation of the propagator

Now we will derive the exact expression of the propagator in terms of path integrals starting from the definition

$$K(x,t,x_0,t_0) = \langle x|\mathrm{e}^{-\frac{i}{\hbar}\mathcal{H}\cdot(t-t_0)}|x_0\rangle \tag{4}$$

Expanding the time evolution into two shorter steps and inserting a 1 gives

$$\begin{aligned} K(x,t,x_0,t_0) &= \langle x|\mathrm{e}^{-\frac{i}{\hbar}\mathcal{H}\cdot(t-t_1)}\mathrm{e}^{-\frac{i}{\hbar}\mathcal{H}\cdot(t_1-t_0)}|x_0\rangle \\ &= \langle x|\mathrm{e}^{-\frac{i}{\hbar}\mathcal{H}\cdot(t-t_1)}\int \mathrm{d}x_1|x_1\rangle\langle x_1|\mathrm{e}^{-\frac{i}{\hbar}\mathcal{H}\cdot(t1-t_0)}|x_0\rangle \\ &= \int \mathrm{d}x_1 K(x,t,x_1,t_1)\cdot K(x_1,t_1,x_0,t_0) \end{aligned} \tag{5}$$

If we do this $N-1$ times and defining a time period of $\tau = (t-t_0)/N$ we get

$$\begin{aligned} K(x,t,x_0,t_0) &= \langle x|(\mathrm{e}^{-\frac{i}{\hbar}\mathcal{H}\cdot\tau})^N|x_0\rangle \\ &= \int\cdots\int \mathrm{d}x_1\cdots\mathrm{d}x_{N-1}K(x,t,x_{N-1},t_{N-1})\cdots K(x_1,t_1,x_0,t_0) \\ &= \int \mathcal{D}x\prod_{i=1}^{N} K(x_{i-1}\to x_i) \end{aligned} \tag{6}$$

where in the last line we set $x = x_N$ and used

$$\int \mathcal{D}x = \prod_{i=1}^{N-1}\int \mathrm{d}x_i \tag{7}$$

In literature $\mathcal{D}$ is often used for the continuous limit

$$\int \mathcal{D}x = \lim_{N\to\infty}\prod_{i=1}^{N}\int \mathrm{d}x_i \tag{8}$$

but since we will, for the actual algorithm, return to a discrete description anyway, we will keep the above description.

Here we can already see the idea of the derivation, since, for a sufficient large N, this integral is equivalent to the sum over all paths and is therefore called a path integral. Now we still have to show the connection between the propagator and the action.

The idea behind the following is to approximate each (short) time evolution step with only

the linear term. For N towards infinity this will converge to the exact result.

$$\begin{aligned} K(x_{i+1}, t_i + \tau, x_i, t_i) &= \langle x_{i+1}| \mathrm{e}^{-\frac{i}{\hbar}\mathcal{H}\cdot\tau} |x_i\rangle \\ &= \langle x_{i+1}| \left(1 - \frac{i}{\hbar}\mathcal{H}\cdot\tau + O(\tau^2)\right) |x_i\rangle \\ &= \langle x_{i+1}|x_i\rangle - \frac{i\tau}{\hbar}\langle x_{i+1}|\mathcal{H}|x_i\rangle + O(\tau^2) \end{aligned} \tag{9}$$

The first bracket of equation (9) is a delta distribution that can be expressed as

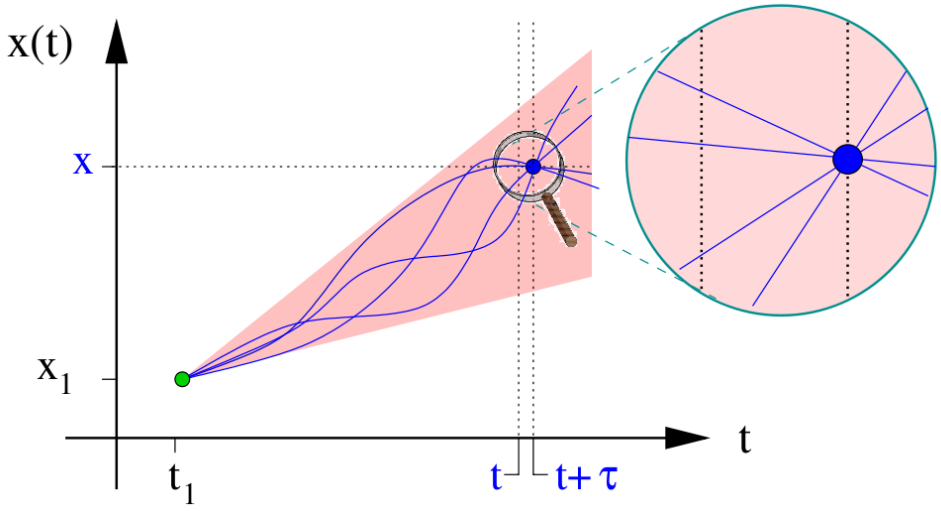

Figure 2: linear approximation for small time steps

$$\langle x_{i+1}|x_i\rangle = \delta(x_{i+1} - x_i) = \int \frac{\mathrm{d}p_i}{2\pi} \mathrm{e}^{\frac{i}{\hbar}p_i(x_{i+1}-x_i)} \tag{10}$$

To evaluate the second term of (9) we have to put in a 1 in form of a sum over momentum states to handle the momentum operator:

$$\begin{aligned} \langle x_{i+1}|\mathcal{H}|x_i\rangle &= \langle x_{i+1}| \left(\frac{\hat{p}^2}{2m} + V(\hat{x})\right) \left(\int \frac{\mathrm{d}p_i}{2\pi} |p_i\rangle\langle p_i|\right) |x_i\rangle \\ &= \int \frac{\mathrm{d}p_i}{2\pi} \left(\frac{p_i^2}{2m} + V(x_{i+1})\right) \langle x_{i+1}|p_i\rangle\langle p_i|x_i\rangle \\ &= \int \frac{\mathrm{d}p_i}{2\pi} \left(\frac{p_i^2}{2m} + V(x_{i+1})\right) \mathrm{e}^{\frac{i}{\hbar}p_i(x_{i+1}-x_i)} \end{aligned} \tag{11}$$

To avoid the asymmetry in this equation x_{i+1} and p_i are usually replaced by an average value

for the time-step in question. The actual choice is arbitrary as long as we take the continuous limit, i.e. letting the time steps (and therefore the spatial steps as well) go to zero. Putting the results (10) and (11) into (9) we obtain

$$\begin{aligned} K(x_{i+1}, t_i + \tau, x_i, t_i) &= \int \frac{\mathrm{d}p_i}{2\pi} \mathrm{e}^{\frac{i}{\hbar} p_i (x_{i+1} - x_i)} - \frac{i\tau}{\hbar} \int \frac{\mathrm{d}p_i}{2\pi} \left(\frac{p_i^2}{2m} + V(x_i) \right) \mathrm{e}^{\frac{i}{\hbar} p_i (x_{i+1} - x_i)} + O(\tau^2) \\ &= \int \frac{\mathrm{d}p_i}{2\pi} \mathrm{e}^{\frac{i}{\hbar} p_i (x_{i+1} - x_i)} \left(1 - \frac{i\tau}{\hbar} \left(\frac{p_i^2}{2m} + V(x_i) \right) + O(\tau^2) \right) \\ &= \int \frac{\mathrm{d}p_i}{2\pi} \mathrm{e}^{\frac{i}{\hbar} p_i (x_{i+1} - x_i)} \mathrm{e}^{-\frac{i\tau}{\hbar} \mathcal{H}(p_i, x_i)} \left(1 + O(\tau^2) \right) \end{aligned} \tag{12}$$

For the last equation we again employed the equivalence between the first two terms and the exponential-function for small τ. With this result we finally can return to equation (6) while using the linear approximation for the velocity $\dot{x}_i = (x_{i+1} - x_i)/\tau$ and finally neglecting the higher orders we obtain

$$K(x, t, x_0, t_0) = \int \mathcal{D}x \prod_{i=0}^{N-1} \left(\int \frac{\mathrm{d}p_i}{2\pi} \right) \mathrm{e}^{\frac{i\tau}{\hbar} \sum_{i=0}^{N-1} (p_i \dot{x}_i - \mathcal{H}(p_i, x_i))} \tag{13}$$

If we put in the Hamiltonian and perform the N gaussian integrals over the p_i we obtain

$$\begin{aligned} K(x, t, x_0, t_0) &= \int \mathcal{D}x \prod_{i=0}^{N-1} \left(\int \frac{\mathrm{d}p_i}{2\pi} \right) \mathrm{e}^{\frac{i\tau}{\hbar} \sum_{i=0}^{N-1} (\frac{p_i^2}{2m} - V(x_i))} \\ &= \left(\frac{m\hbar}{2\pi i \tau} \right)^{N/2} \int \mathcal{D}x \ \mathrm{e}^{\frac{i\tau}{\hbar} \sum_{i=0}^{N-1} (\frac{p_i^2}{2m} - V(x_i))} \end{aligned} \tag{14}$$

Here the exponent is equal to the discretised integral of the Lagrangian over time (again this is only valid for small τ), so we can replace it by the action

$$K(x, t, x_0, t_0) = \left(\frac{m\hbar}{2\pi i \tau} \right)^{N/2} \int \mathcal{D}x \ \mathrm{e}^{\frac{i}{\hbar} S[x]} \tag{15}$$

where S depends on all $N + 1$ coordinates (as well as the velocities at these positions) from x_0 to x. So finally we showed that (2) is correct and even got the prefactor. The above derivation largely followed the one of Feynman's original paper. [5]

Today the Path Integral formalism is intensively used not only in particle physics and Quantum Monte Carlo Simulations. It provides clear and intuitive explanations of various quantum effects, e.g. the Aharonov-Bohm effect, following from this particle statistics (anyons) up to the relation between magnetic monopoles and charge quantisation [11].

2.2 From the propagator to the density matrix

As we will see in this section the above derived propagator is closely connected to statistical mechanics, although it describes dynamics. First we should remember the central quantity of quantum statistics, the density matrix

$$\rho = \sum_i |i\rangle\langle i| \cdot p(i) \tag{16}$$

which gives, for the canonical ensemble

$$\rho = \sum_i |i\rangle\langle i| \cdot \mathrm{e}^{-\beta E_i} \tag{17}$$

with $\beta = 1/(k_B T)$. Now we start again from the definition of the propagator (4)

$$\begin{aligned} K(x,t,x_0,t_0) &= \langle x|\mathrm{e}^{-\frac{i}{\hbar}\mathcal{H}\cdot(t-t_0)}|x_0\rangle \\ &= \langle x|\mathrm{e}^{-\frac{i}{\hbar}\mathcal{H}\cdot(t-t_0)}\sum_i |i\rangle\langle i|x_0\rangle \\ &= \sum_i \langle x|i\rangle\langle i|x_0\rangle \mathrm{e}^{-\frac{i}{\hbar}E_i\cdot(t-t_0)} \qquad (18) \\ \rho(x_0,x) = \langle x|\rho|x_0\rangle &= \sum_i \langle x|i\rangle\langle i|x_0\rangle \mathrm{e}^{-\beta E_i} \qquad (19) \end{aligned}$$

Obviously the last to right hand sites are equal, if $i(t-t_0)/\hbar = \beta$. So we can express the density matrix with the propagator (we can set $t_0 = 0$ since our Hamiltonian is time independent and therefore the system time-invariant)

$$\rho(x_0,x) = K(x, -i\beta/\hbar, x_0, 0) \tag{20}$$

To express this with an actual path integral we have to go back to equation (14) and replace τ by

$$\tau = \frac{t-t_0}{N} = \frac{-i\beta\hbar}{N} \tag{21}$$

yielding

$$\rho(x_0,x) = \left(\frac{m\hbar}{2\pi i\tau}\right)^{N/2} \int \mathcal{D}x \; \mathrm{e}^{\frac{\beta}{N}\sum_{i=0}^{N-1}(\frac{p_i^2}{2m} - V(x_i))} \tag{22}$$

Since a velocity, while evaluating a propagator in imaginary time, isn't well defined, we replace p by

$$p = m\frac{\Delta x}{\tau} = im\frac{\Delta x N}{\beta\hbar} \tag{23}$$

and therefore reaching our final result

$$\rho(x_0, x) = \left(\frac{m\hbar}{2\pi i\tau}\right)^{N/2} \int \mathcal{D}x \; \mathrm{e}^{-\sum_{i=0}^{N-1}\left(\frac{m\Delta x_i^2 N}{2\beta\hbar^2} + \frac{\beta}{N}V(x_i)\right)} \tag{24}$$

Now we can, theoretically, calculate the elements of the density matrix, particularly the diagonal elements by setting $x = x_0$, by evaluating the path integral. This is, however, still impractical since one would need infinite computing power to calculate the precise values of the integrals. To solve this problem and create an algorithm that computes a good approximation we need to understand the principle of so called Monte Carlo Simulations.

2.3 Monte Carlo simulations

The Monte Carlo Method makes it possible to calculate many kinds of integrals. This is done with, as the name suggests, a probability element. A simple example is the Integral over an arbitrary function

$$\int_0^1 f(x) \approx \frac{1}{N}\sum_{i=1}^{N} f(x_i) \tag{25}$$

This equation is true, if the x_i are equally distributed between 0 and 1. One can come as close to the true value as possible raising the N sufficiently.

Another possibility is shown with the next example in which we describe an algorithm to compute π. One has to generate equally distributed coordinate pairs in a 1×1 square and check

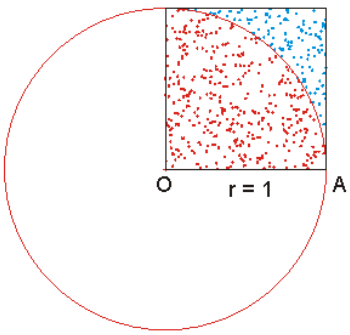

Figure 3: calculating π with Monte Carlo simulation

whether they lie in the circle or not. The ratio between the number of pairs in the circle and the total number will give $\pi/4$ if one does enough steps.

2.4 Metropolis algorithm

The above described method is in general valid for any integral, but in some cases somehow impracticable. If one has for example an integrand weighted with a density probability ρ like

$$\langle A \rangle = \int \mathrm{d}x \rho(x) A(x) \tag{26}$$

(e.g. the mean value of A over configuration space) the so called Metropolis algorithm is much more efficient since it doesn't waste time sampling through regions of configuration space in which the system hardly is found and therefore the probability is extremely low (and so the contribution to the integral is extremely small). It samples through the coordinate space in question in the following way:

1. Create a random start point x_0 (here the index refers to the Metropolis step rather then the timeslice as above).

2. Evaluate function at this point.

3. Create a new point
$$x' = x_i + r \cdot \Delta x \tag{27}$$
where r is a random number $r \in [-1, 1]$ and Δx a stepwidth that has to be chosen appropriately (see next step).

4. Set the next point
$$x_{i+1} = \begin{cases} x', & \text{if } \frac{\rho(x')}{\rho(x_i)} > s \\ x_i, & \text{otherwise} \end{cases} \tag{28}$$
(where $s \in [0, 1]$ is a random number) and go back to 2. until N is reached.

The stepwidth Δx of step 3 has to be chosen in a way, that the average acceptance rate in step 4 (i.e. $x_{i+1} = x'$) is around 50%. This assures, that all important regions of the configuration space are sampled and no computing power is wasted elsewhere. An extension to higher dimensions is easily possible by doing the same thing for the other dimensions and choosing the dimension in which to do a trialmove randomly.

3 Numerical approach

Now we are able, when putting together all the parts of the previous paragraph, to actually analyse the statistics of a quantum mechanical system. What we want is to calculate expectation

values like with equation (26) using the metropolis algorithm. The probability density ρ we obtain from the density matrix, which we can, due to equation (24), express as a path integral. Because of the discrete and finite nature of computers, we have to use a finite N and discretise the integrals to sums over all paths we are sampling through. It is crucial, that we are not only sampling a single vector, but a whole chain of N such vectors. This is due to the way we describe our system. It is no longer represented by a wavefunction in space-time, but by a (weighted) sum over all paths through space-time.

3.1 Monte Carlo step

A single Monte Carlo or, more correctly, Metropolis step, roughly described in section 2.4, looks as follows.

We choose from our multidimensional chain (number of particles $\times$ number of timeslices (N) $\times$ number of spatial dimensions) a random particle, timeslice and direction. Now all parts of the action containing the position of that part of the chain are calculated and stored. The next step is to perform a trial move, i.e. change the position by a random value (see point 3 of section 2.4). Again the parts of the action, that just have changed are calculated. By comparing the new and old value of the action following point 4 the trial move is either accepted or not. In both cases the quantities one is interested in are now evaluated and stored in order to calculate the averages at the end of the whole run.

3.2 Calculating the action

In order to determine what actually needs to be calculated one should have a look back at equation (24). One finds that the density matrix factorises in the contribution of every small time-step. So one just has to take the step from and towards the neighbouring slices, respectively, of the one in question into account, since the contributions of all other steps would cancel out each other when applying (28).

Denoting the coordinate we have chosen x_i (with the index referring to the timeslice), we have to calculate

$$\rho(x_i) = \rho(x_{i-1}, x_i) \cdot \rho(x_i, x_{i+1}) \propto \mathrm{e}^{-\left(\frac{m(x_i - x_{i-1})^2 N}{2\beta\hbar^2} + \frac{\beta}{N} V(\tilde{x}_{i-1})\right)} \cdot \mathrm{e}^{-\left(\frac{m(x_{i+1} - x_i)^2 N}{2\beta\hbar^2} + \frac{\beta}{N} V(\tilde{x}_i)\right)} \tag{29}$$

We remember that the $\tilde{x}_i$ in the potential are an average value between x_i and x_{i+1}, but that the choice is, for small τ, actually arbitrary. So for simplicity we choose $\tilde{x}_{i-1} = x_i$ and $\tilde{x}_i = x_{i+1}$.

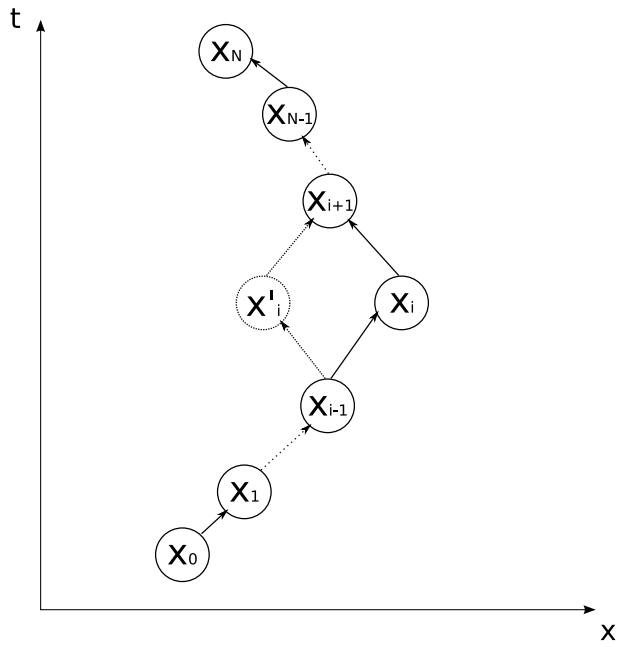

Figure 4: trial move for single particle path at x_i

We can rewrite (29)

$$\rho(x_i) \propto \mathrm{e}^{-\frac{\beta}{N}V(x_i)}\mathrm{e}^{-\frac{\beta}{N}V(x_{i+1})}\left(\mathrm{e}^{-\frac{m(x_i-x_{i-1})^2N}{2\beta\hbar^2}}\cdot\mathrm{e}^{-\frac{m(x_{i+1}-x_i)^2N}{2\beta\hbar^2}}\right) \tag{30}$$

In order to employ the Metropolis algorithm one has now just to calculate the ratio of this quantity after and before the trial move. Since only x_i was changed the potential parts of x_{i+1} will cancel out each other. So this choice will, especially for the (anti-)symmetric case, make life much easier.

$$\frac{\rho(x_i')}{\rho(x_i)} = \mathrm{e}^{-\frac{\beta}{N}(V(x_i')-V(x_i))}\cdot\frac{\mathrm{e}^{-\frac{m(x_i'-x_{i-1})^2N}{2\beta\hbar^2}}\cdot\mathrm{e}^{-\frac{m(x_{i+1}-x_i')^2N}{2\beta\hbar^2}}}{\mathrm{e}^{-\frac{m(x_i-x_{i-1})^2N}{2\beta\hbar^2}}\cdot\mathrm{e}^{-\frac{m(x_{i+1}-x_i)^2N}{2\beta\hbar^2}}} \tag{31}$$

As it stands this can be further simplified, but for better comparison to the extension described in the next section we let it stay as it is.

Until this point the indices referred to the timeslice and dashed quantities are those after the trial move was performed. Since in the next paragraph contributions to the density matrix with mixed particle numbers will occur and to keep consistency we will use upper indices for the particle in question.

3.3 Symmetrisation

Since in this project indistinguishable bosons are the matter of interest one has to take the statistical interaction into account. For bosons this can be obtained by symmetrising the many particle wavefunction, i.e. the wavefunction has to be invariant when swapping two particle's coordinates. For a two particle system this can be achieved with

$$\Psi(x^1, x^2) = \frac{1}{\sqrt{2}} \left(\phi_1(x^1)\phi_2(x^2) + \phi_1(x^2)\phi_2(x^1)\right) \tag{32}$$

where for fermions one would have to replace the plus by a minus. For n particles this can be expressed by the permanent of the Slater-matrix

$$\Psi(x^1, x^2, \ldots, x^n) = \frac{1}{\sqrt{n!}} \cdot perm \begin{pmatrix} \phi_1(x^1) & \phi_1(x^2) & \cdots & \phi_1(x^n) \\ \phi_2(x^1) & \phi_2(x^2) & \cdots & \phi_2(x^n) \\ \vdots & \vdots & \ddots & \vdots \\ \phi_n(x^1) & \phi_n(x^2) & \cdots & \phi_n(x^n) \end{pmatrix} \tag{33}$$

The permanent of a matrix is similar to the determinant, except the alternating sign is dropped. Since we are in the regime of small steps in time while approximating the wavefunction with a sum over classical paths, our wavefunctions ϕ_i are localised and so (32) can be rewritten:

$$|\Psi\rangle = \frac{1}{\sqrt{2}} \left(|x^1\rangle|x^2\rangle + |x^2\rangle|x^1\rangle\right) \tag{34}$$

Recall the definition of the propagator (4), that it is the amplitude of finding a particle at (x, t) after it started at (x_0, t_0). Now we have to adapt the formulation, since we have two particles that are indistinguishable. The propagator is the amplitude of finding the system in a uniform superposition of the two possibilities of distributing the particles over x^1 and x^2 at time t after they have started in a similar superposition, but with coordinates x_0^1 and x_0^2 at time t_0. This yields for one time step

$$\begin{aligned} K(x_{i+1}^1, x_{i+1}^2, \tau, x_i^1, x_i^2, 0) &= \langle\Psi'|\mathrm{e}^{-\frac{i\tau}{\hbar}\mathcal{H}}|\Psi\rangle \\ &= \frac{1}{\sqrt{2}} \left(\langle x_{i+1}^1|\langle x_{i+1}^2| + \langle x_{i+1}^2|\langle x_{i+1}^1|\right) \mathrm{e}^{-\frac{i\tau}{\hbar}\mathcal{H}} \frac{1}{\sqrt{2}} \left(|x_i^1\rangle|x_i^2\rangle + |x_i^2\rangle|x_i^1\rangle\right) \\ &= \frac{1}{2}(\langle x_{i+1}^1|\langle x_{i+1}^2|\mathrm{e}^{-\frac{i\tau}{\hbar}\mathcal{H}}|x_i^1\rangle|x_i^2\rangle + \langle x_{i+1}^1|\langle x_{i+1}^2|\mathrm{e}^{-\frac{i\tau}{\hbar}\mathcal{H}}|x_i^2\rangle|x_i^1\rangle \\ &\quad + \langle x_{i+1}^2|\langle x_{i+1}^1|\mathrm{e}^{-\frac{i\tau}{\hbar}\mathcal{H}}|x_i^1\rangle|x_i^2\rangle + \langle x_{i+1}^2|\langle x_{i+1}^1|\mathrm{e}^{-\frac{i\tau}{\hbar}\mathcal{H}}|x_i^2\rangle|x_i^1\rangle) \end{aligned} \tag{35}$$

Again we choose the potential to be evaluated at the mid points and since it doesn't depend on the order of the particle, it is the same in all summands. That leaves the kinetic energies to be evaluated. They consist now of two factorising operators, each acting on different sub-Hilbert spaces and can therefore be calculated separately. For the first summand the derivation is

$$\begin{aligned}\langle x^1_{i+1}|\langle x^2_{i+1}|\mathrm{e}^{-\frac{i\tau}{\hbar}\mathcal{H}}|x^1_i\rangle|x^2_i\rangle &= \langle x^1_{i+1}|\langle x^2_{i+1}|\mathrm{e}^{-\frac{i\tau}{\hbar}\mathcal{T}_1}\cdot\mathrm{e}^{-\frac{i\tau}{\hbar}\mathcal{T}_2}|x^1_i\rangle|x^2_i\rangle \\ &= \langle x^1_{i+1}|\mathrm{e}^{-\frac{i\tau}{\hbar}\mathcal{T}_1}\langle x^2_{i+1}|x^1_i\rangle\mathrm{e}^{-\frac{i\tau}{\hbar}\mathcal{T}_2}|x^2_i\rangle \qquad (36)\end{aligned}$$

The bra and ket vectors in the middle of (36) belong to different sub-Hilbert spaces and therefore can be swapped

$$= \langle x^1_{i+1}|\mathrm{e}^{-\frac{i\tau}{\hbar}\mathcal{T}_1}|x^1_i\rangle\langle x^2_{i+1}|\mathrm{e}^{-\frac{i\tau}{\hbar}\mathcal{T}_2}|x^2_i\rangle \propto K(x^1_{i+1},\tau,x^1_i,0)\cdot K(x^2_{i+1},\tau,x^2_i,0) \qquad (37)$$

(the last $\propto$ is due to the potential part we neglected before and now put in again)

With this result and again the fact that the particles are indistinguishable we find that the first and last summand as well as the second and third of (35) will give the same and so we end up with

$$K(x^1_{i+1},x^2_{i+1},\tau,x^1_i,x^2_i,0) = K(x^1_{i+1},\tau,x^1_i,0)\cdot K(x^2_{i+1},\tau,x^2_i,0)+K(x^2_{i+1},\tau,x^1_i,0)\cdot K(x^1_{i+1},\tau,x^2_i,0) \qquad (38)$$

That is exactly what one expects intuitively. Due to the indistinguishability both possible paths are realised simultaneously and their probabilities just add.

If we again use (20) and go over to the density matrix we obtain

$$\rho(x^1_i,x^2_i,x^1_{i+1},x^2_{i+1}) = \rho(x^1_i,x^1_{i+1})\cdot\rho(x^2_i,x^2_{i+1})+\rho(x^1_i,x^2_{i+1})\cdot\rho(x^2_i,x^1_{i+1}) \qquad (39)$$

The derivation above can be generalised for n particles similarly to (33):

$$\rho(x^1_i,x^2_i,\ldots,x^n_i,x^1_{i+1},x^2_{i+1},\ldots,x^n_{i+1}) = perm\begin{pmatrix}\rho(x^1_i,x^1_{i+1}) & \rho(x^1_i,x^2_{i+1}) & \cdots & \rho(x^1_i,x^n_{i+1})\\ \rho(x^2_i,x^1_{i+1}) & \rho(x^2_i,x^2_{i+1}) & \cdots & \rho(x^2_i,x^n_{i+1})\\ \vdots & \vdots & \ddots & \vdots\\ \rho(x^n_i,x^1_{i+1}) & \rho(x^n_i,x^2_{i+1}) & \cdots & \rho(x^n_i,x^n_{i+1})\end{pmatrix} \qquad (40)$$

To calculate all parts of the density matrix that change when doing a trial move on x^j_i, illustrated in Fig. 5 for two particles, we have to calculate four such permanents, since we need two transitions, one from the previous and one towards the next timeslice, each to be calculated before and after the trial move.

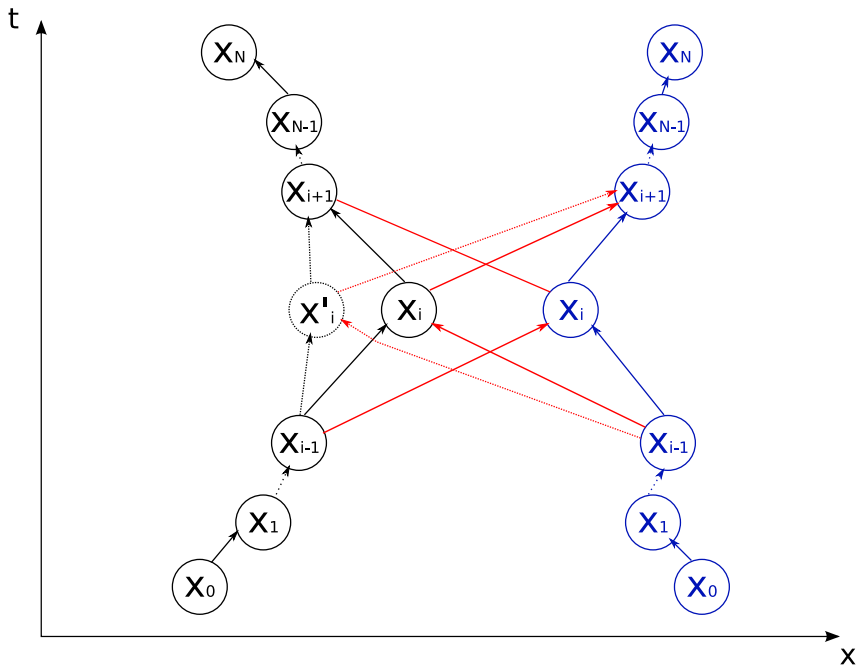

Figure 5: trial move for a two particle path at x_i

$$\frac{\rho(x_i^{j\prime})}{\rho(x_i^j)} = \frac{\rho(x_i^{j\prime}, t-\tau, t)\cdot\rho(x_i^{j\prime}, t, t+\tau)}{\rho(x_i^j, t-\tau, t)\cdot\rho(x_i^j, t, t+\tau)} \tag{41}$$

Here each ρ refers to a permanent of single particle density matrices. Since permanents are linear in every row and column, respectively and we chose the position to evaluate the potential appropriate, we can, in the numerator, take out $2n$ potential parts of which $2n-1$ will cancel out with the corresponding matrix in the denominator as seen before in (31). This simplifies the matrix of equation (40) to the "kinetic matrix" T with only the kinetic parts of the density left. Actually the ρ's in the upper equation do not only depend on x_i^j and $x_i^{j\prime}$, respectively, but also on all other coordinates of the three timeslices that have to be evaluated, due to interaction potentials. Now we should use $\vec{x}$ and $\vec{x}'$, containing all necessary coordinates and the latter one with $x_i^{j\prime}$ rather than x_i^j. Using this notation we end up with

$$\frac{\rho(\vec{x}')}{\rho(\vec{x})} = \mathrm{e}^{-\frac{\beta}{N}(V(\vec{x}')-V(\vec{x}))}\cdot\frac{perm(T(\vec{x}', t-\tau, t))\cdot perm(T(\vec{x}', t, t+\tau))}{perm(T(\vec{x}, t-\tau, t))\cdot perm(T(\vec{x}, t, t+\tau))} \tag{42}$$

3.3.1 Calculating the permanent

As explained above it is necessary to calculate the permanent of the Slater-matrix in order to satisfy the bosonic symmetrisation relations. In my code an algorithm due to the so called

Ryser-formula (Eqn. 43) [13] is employed. It calculates the permanent of a $(n \times n)$ matrix A as follows:

$$perm(A) = \sum_{S \subseteq \{1,\ldots,n\}} (-1)^{|S|} \prod_{i=1}^{n} \sum_{j \notin S} a_{ij} \tag{43}$$

Here the first sum is over all $(n \times k)$ submatrices $(k \leq n)$ of A. There are 2^n possibilities of forming such a submatrix, what gives a (best case) total computational cost of $O(2^n \cdot n)$. However, the algorithm in my code has a cost of $O(2^n \cdot n^2)$.

Algorithms based on this formula are the so far fastest known ways of calculating a permanent for general matrices. There is, however, another way of including symmetrisation relations, allowing a significant higher number of particles being simulated. I will come back to this in the discussion.

3.4 Calculating the total energy

One of the main quantities of interest in ground state simulations like described above, is the ground state energy of the system. It consists of a kinetic and a potential part. Because we are, in PIQMC simulations, usually only sampling through real space, but not momentum space, evaluation the potential energy is simple, but the kinetic part is not. We obtain the kinetic part of the action by the ratio of spatial- and time-step, but since our time is complex, we cannot use it to calculate an actual physical quantity. The solution to that problem is the *Virial Theorem*, connecting average kinetic energy to the average potential energy. This is perfectly suitable, since in Monte Carlo simulations one can calculate only averages anyway. The derivation of the theorem is presented in the next paragraph.

3.4.1 The Virial theorem

We can write the kinetic energy as a function of momentum and velocity of all particles and rewrite it employing the product rule of derivation.

$$2T = \sum_i \vec{p}_i \cdot \vec{v}_i = \frac{\mathrm{d}}{\mathrm{d}t} \left(\sum_i \vec{p}_i \cdot \vec{r}_i \right) - \sum_i \vec{r}_i \cdot \dot{\vec{p}}_i \tag{44}$$

Now we will calculate the average with respect to time of both sides. It is defined as

$$\bar{f} = \lim_{\tau \to \infty} \frac{1}{\tau} \int_0^\tau f(t) \mathrm{d}t \tag{45}$$

If $f(t)$ can be expressed as the time derivative of a bounded function $F(t)$, we find the average of that function vanishing

$$\bar{f} = \lim_{\tau\to\infty} \frac{1}{\tau} \int_0^\tau \frac{\mathrm{d}F(t)}{\mathrm{d}t} \mathrm{d}t = \lim_{\tau\to\infty} \frac{F(\tau) - F(0)}{\tau} = 0 \tag{46}$$

If we assume a system in a finite region of space with finite velocities, the first summand of (44) is bounded and therefore its average vanishes. Using this and the Newton's equation of motion as well as the definition of force

$$\dot{\vec{p}}_i = \vec{F}_i = -\frac{\partial V}{\partial \vec{r}_i} \tag{47}$$

we obtain

$$2\bar{T} = \overline{\sum_i \vec{r}_i \cdot \frac{\partial V}{\partial \vec{r}_i}} \tag{48}$$

where we used the notation $\frac{\partial V}{\partial \vec{r}} = \frac{\partial V}{\partial x}\vec{e}_x + \frac{\partial V}{\partial y}\vec{e}_y + \frac{\partial V}{\partial z}\vec{e}_z$ with the unit vectors $\vec{e}_i$.

We can see that, as long as the gradient of the potential can be derived, one can calculate the total (average) energy of the system $\bar{E} = \bar{T} + \bar{V}$.

3.5 Program structure

Now as we have obtained all pieces that have to be included into the code we can have a look onto the full structure of the code, summarised in the appendix C.

The code basically starts with the creation of a three dimensional array for storing the path (recall: number of particles × number of timeslices (N) × number of spatial dimensions). Then the actual path, i.e. the values for all points in the chain, is created wit more or less arbitrary. However, it turned out that initialising the different particles side by side in certain regions that do not overlap is reasonable. This is due to the fact, that if to particles are almost coinciding, the implemented *Lennard-Jones* repulsion raises the potential energy enormously which can cause large numerical errors. Furthermore initialising paths going around the ring several times can, if an external potential is applied, cause convergence problems. Afterwards the total energy of the initial path is calculated.

The next step is the initialisation of the system. This is necessary in order to bring the random start path into the thermo dynamic equilibrium before starting the evaluation of quantities. This is done without using symmetrisation due to the fact, that the initial path isn't necessarily in the regime appropriate for the algorithm, for example it might have time steps with extreme high kinetic energies, what would cause the result of (42) to be $0/0 = \mathrm{NaN}$. The algorithm would accept steps that shouldn't be accepted and therefore won't reach thermal equilibrium. The code performs 10,000 initial Monte Carlo steps per particle, timeslice and dimension.

After initialisation the code tries to find the optimal stepwidth for every dimension. This is done by trying to get the acceptance rate as close as possible to 50%, as mentioned in section 2.4. A search algorithm is applied, evaluating each stepwidth with a thousand Monte Carlo steps per particle and timeslice and then raising or lowering the stepwidth until the difference to 50% acceptance rate is smaller than a defined value. These steps are already symmetrised. In order to achieve the symmetric sampling efficiently, a second three dimensional array is introduced which corresponds to the matrix T of equation (42), but stored for all transitions along the path. After a trial move only the values that have changed are recalculated.

In order to keep track of the energy during calculation it is not necessary to calculate the total energy of the whole path after every accepted trial move. It is only necessary to calculate those parts of the energy that are influenced by the position in question before and, if accepted, after the trial move. Now only the difference has to be added to the total energy, once evaluated at the beginning.

4 Results

Following sections results obtained with the above described code will be presented. Starting with the verification of the code simulating simple single particle systems, going over to many particle bose systems to finally bosons with associated dipole moment. The basic system in which the particles are simulated is a ring with a radius of several microns, i.e. a one dimensional system with periodic boundary conditions. The particles used were given the mass of rubidium atoms (e.g. used in [12]) $m = 1.4192260 \cdot 10^{-25}$kg.

4.1 Verification of the code

In the very beginning of the project the correctness of the code was tested with the most simple, nontrivial system, the harmonic oscillator. This was mainly done to verify the code and to get used to the various parameters the algorithm needs and their influence on convergence or even the result, e.g. on the ground state energy. The outcome of this first part of the project is that it finally worked and we were able to obtain the correct (analytical) result. Going ahead to the atomic ring we encountered the problem, that there are no potentials for which analytical results exist. In order to verify this extension of the code the resulting ground state energy is compared with the result of a matlab program that solves the problem by discretising the Schrödinger equation.

An external potential of the form

$$V^{ext} = V_0^{ext} \cdot (1 + \cos\varphi) \tag{49}$$

was used with $V_0^{ext} = 10^{-10}$eV. The radius was set to $R = 10\mu m$.

The following plot (fig. 6) shows how the ground state energy behaves when lowering the temperature as well as the energy obtained from the matlab code.

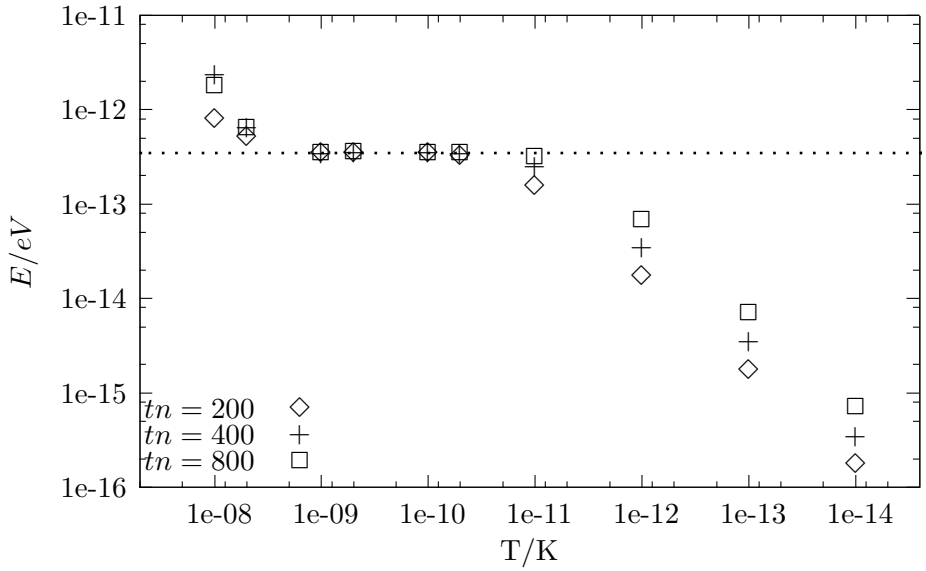

Figure 6: Energy of a single boson in an external potential with $V_0^{ext} = 10^{-10}eV$ for three different numbers of timeslices. Number of performed Monte Carlo steps was $2 \cdot 10^9$. The dotted line marks the result obtained with a matlab code ($E = 3.494 \cdot 10^{-13}eV$).

Unfortunately it is numerically impossible to simulate the system with temperatures much higher than $10^{-7}K$ due to the already mentioned problem of getting NaNs for the metropolis algorithm for to high energies. Already for $10^{-8}K$ even 2 trillion steps are not enough to sample a symmetric gaussian wavefunction.

On the other hand too low temperatures cause the sampled energy to decrease linearly, what is a well known phenomenon in PIQMC. This decrease can be delayed by increasing the number of timeslices (i.e. the "length" of the chain representing the path).

Evidence that one really has to be in such a low temperature regime can be obtained by analysing the thermal wavelength

$$\lambda_T = \frac{h}{\sqrt{2\pi m k_B T}} \tag{50}$$

A previous project observed quantum effects with electrons of (reduced) mass of order 10^{-32} at distances of $\sim 10nm$ at $\sim 10K$. Now we have a seven orders of magnitude higher mass and a length scale of $\sim 10\mu m$. Putting this into the expression for λ_T one can see that temperatures of order $10^{-9}K$ are adequate. Also experimental realisations of atomic rings work with

temperatures down to $10nK$.

What one can see from the plot, is the energy goes down to the real value. The larger the number of timeslices, the longer it stays at this level. We can conclude that it is possible to obtain the ground state properties over a sufficient range of temperature of at least one order of magnitude.

A verification of not only a single particle system, but an antisymmetrised two particle system was also realised by comparing the obtained energy with the sum of the energies of the first two states, given by the matlab code. The parameters used were $V_0^{ext} = 10^{-10}$eV and $R = 10\mu m$ and the permanent was replaced by a function calculating the determinant instead.

$$\begin{aligned} E_{matlab} &= 1.397 \cdot 10^{-12}\text{eV} \\ E_{PIQMC} &= 1.370 \cdot 10^{-12}\text{eV} \end{aligned}$$

This corresponds to an error of less than 2% and gives strong reliability to the (anti-)symmetrisation part of the code.

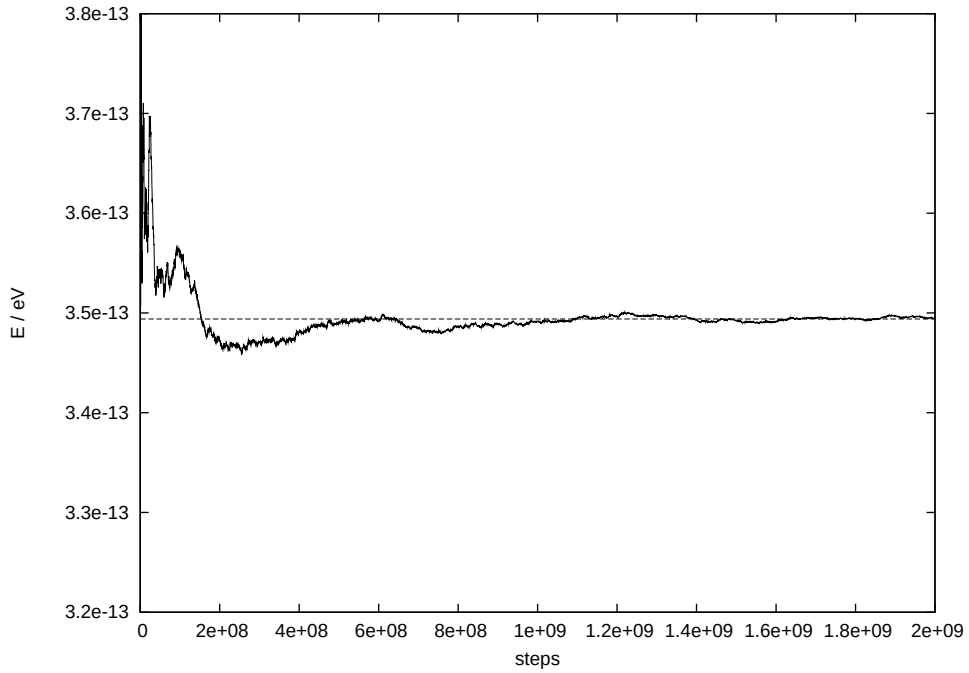

Figure 7: The averaged energy against the number of performed Monte Carlo steps recorded during a simulation with $2 \cdot 10^9$ steps at $0.5nK$ for a single boson in the external potential.

How fast a simulation converges to an equilibrium is shown in figure 7. In the simulation in which this graph was obtained, 200 timeslices were used. One can see, that for more than 10^9

steps the reached value is already a adequate approximation. Apparently the deviation becomes much smaller for even higher numbers towards $2 \cdot 10^9$. For the following sections it should be kept in mind, this number needs to be increased with the number of dimensions, the number of particles and the number of timeslices. So sometimes a satisfying number of steps couldn't be reached due to extremely increasing run times.

4.2 Non-interacting indistinguishable bosons

The next step was to realise simulations with more particles and included symmetrisation. The main problem here is the exponential increase in computing resources necessary for a sufficient high number of steps (see section 3.3.1). This is pointed out in figure 8, where the used cpu-time is plotted against the number of particles for the symmetrised as well as for the non-symmetrised case.

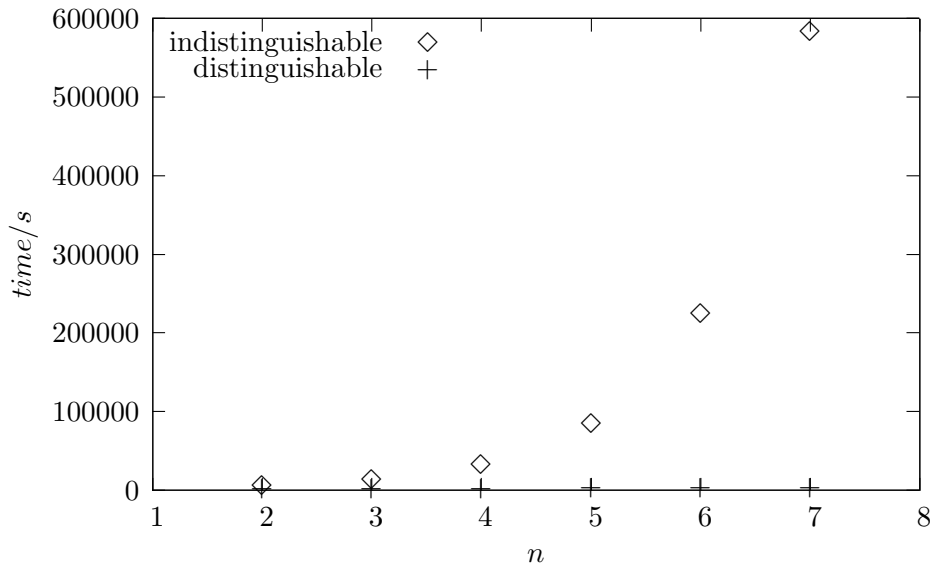

Figure 8: Used CPU time against the number of simulated particles. 10^9 Monte Carlo steps were performed.

The main feature that one would like to observe is the developing difference between the two cases with increasing particle number due to Bose-Einstein condensation. Since observable differences in energy aren't expected we focused on correlation quantities like the pair distance distribution. Here the development of a hump at zero distance can be expected. Figure 9 was obtained by simulating 10 distinguishable and indistinguishable bosons, respectively in the external potential already used in the previous section.

However, our simulations don't show such a feature. The two distance distributions of

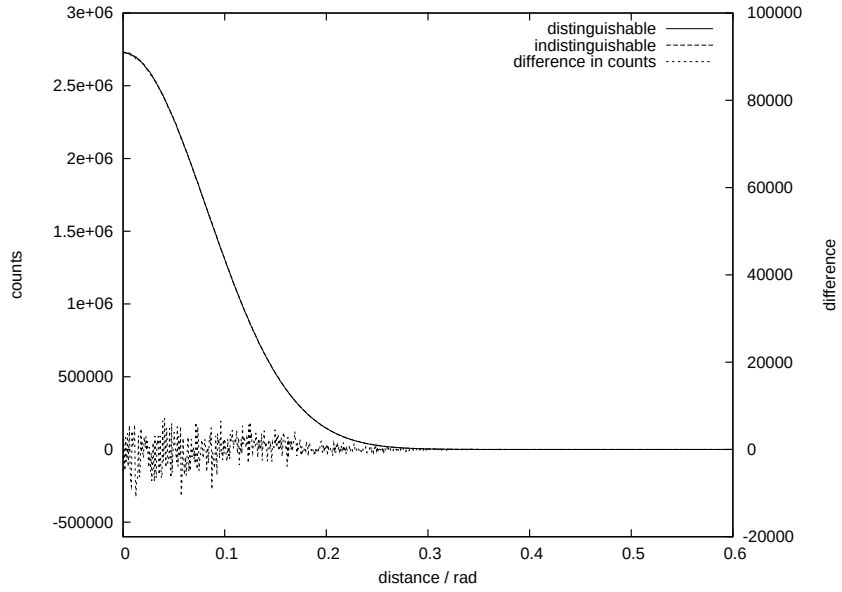

Figure 9: Comparison of the distributions of the distance between two particles for distinguishable and indistinguishable bosons. Obtained from a simulation of 10 bosons in $5 \cdot 10^7$ steps at $0.1nK$.

distinguishable and indistinguishable bosons don't show a significant difference to each other. The plotted difference between the counts of the two simulations is increasing towards zero distance, but equally distributed vertical around zero counts, what is a known effect in PIQMC.

Another quantity related to condensation effects and observed by us is the so called connected part of the correlation function. For a somehow distributed physical quantity r it is defined as follows [9]

$$\langle r_i r_j \rangle_{conn} = \langle r_i r_j \rangle - \langle r_i \rangle \langle r_j \rangle \tag{51}$$

where $\langle\ \rangle$ stands for the ensemble average.

It is positive if r_i and r_j are correlated, zero if uncorrelated and negative if anticorrelated. The next plot (figure 10) shows this connected part against the number of particles again for distinguishable and indistinguishable particles.

One can see a significant increase in the correlation from 6 particles on, what may indicate an inceptive condensation. If this trend is continued for higher particle numbers couldn't be clarified, since the enormous runtime for increasing particle numbers only allowed to perform $5 \cdot 10^7$ steps in a reasonable amount of time. The results from these simulations partially confirmed the observed trend, but showed a big uncertainty hence reliability is quite poor. Nevertheless, the obtained reliable data motivates to try simulating higher numbers of particles

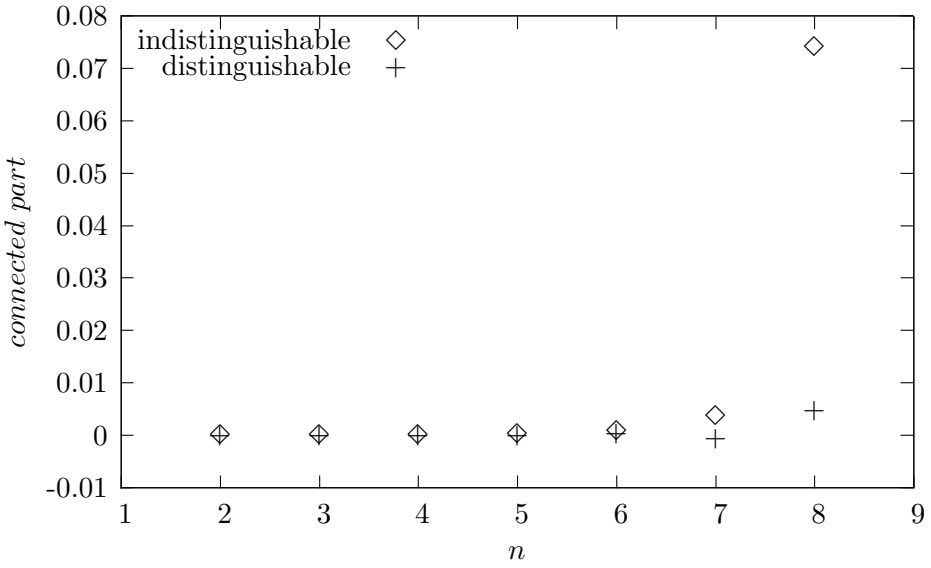

Figure 10: The connected part $\langle r_i r_j \rangle_{conn}$ against number of particles for both cases. Obtained from a simulation of up to 8 particles with 10^9 steps at $0.1nK$.

(see discussion).

4.3 Interacting indistinguishable bosons - the Tonks-Girardeau gas

To point out the effect of a repulsive hard core potential on a bose gas we will compare this system with the non-interacting bose gas, to see the fundamental change of behaviour, and to a fermi gas of non-interacting fermions, to see the similarities between these two systems. This is realised by simulations with two particles to keep clearness. The repulsive potential used in these simulations is the repulsive part of the Lennard-Jones potential.

$$V^{LJ} = \frac{1}{2} V_0^{LJ} \sum_i^n \sum_{j \neq i}^n \left(\frac{\sigma}{d_{ij}} \right)^{12} \tag{52}$$

where σ is a parameter for the effective range of the repulsion. V_0^{LJ} is the strength of the potential usually chosen to be equal to the strength of the external potential $V_0^{LJ} = V_0^{ext} = 10^{-12}$eV (here).

In the following two plots (figures 11-12) the distribution of the particles on the ring as well as the pair distance distribution between the two particles for the three cases are presented. For the interacting case $\sigma = R/15$ was used.

The fundamental change in behaviour of the bose gas is most obvious in the distance distri-

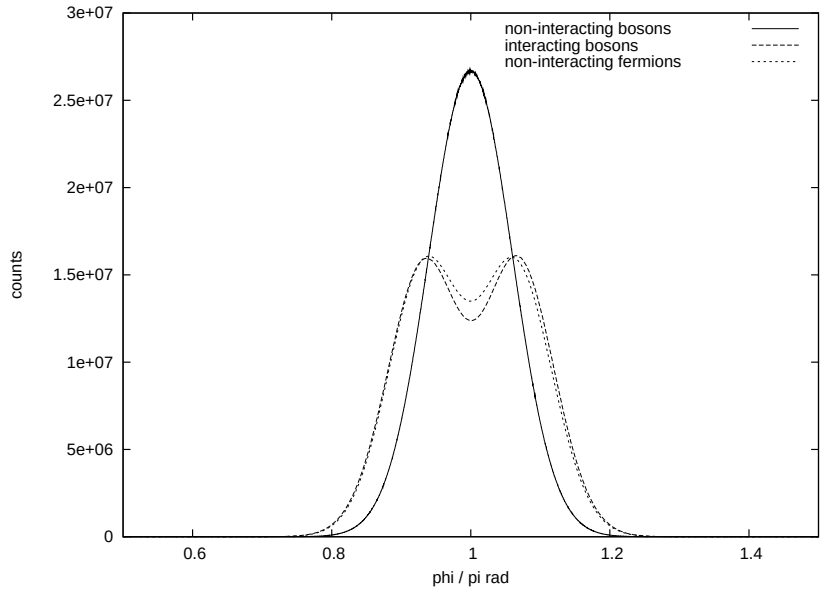

Figure 11: The particle distributions of indistinguishable bosons with and without interaction as well as indistinguishable fermions without interaction. All simulated with $2 \cdot 10^9$ steps at $0.1nK$.

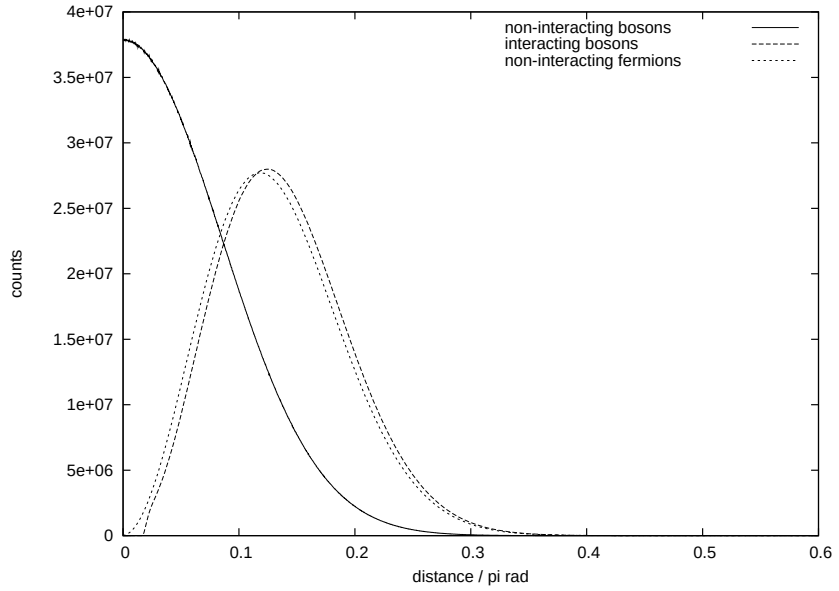

Figure 12: The pair distance distributions of indistinguishable bosons with and without interaction as well as indistinguishable fermions without interaction. All simulated with $2 \cdot 10^9$ steps at $0.1nK$.

bution, changing from the maximum value at $d = 0$ to zero counts at this distance. Furthermore one can see a transition from a single peak distribution to the development of two clearly distinguishable maxima. This transition is pointed out in greater detail in figure 13.

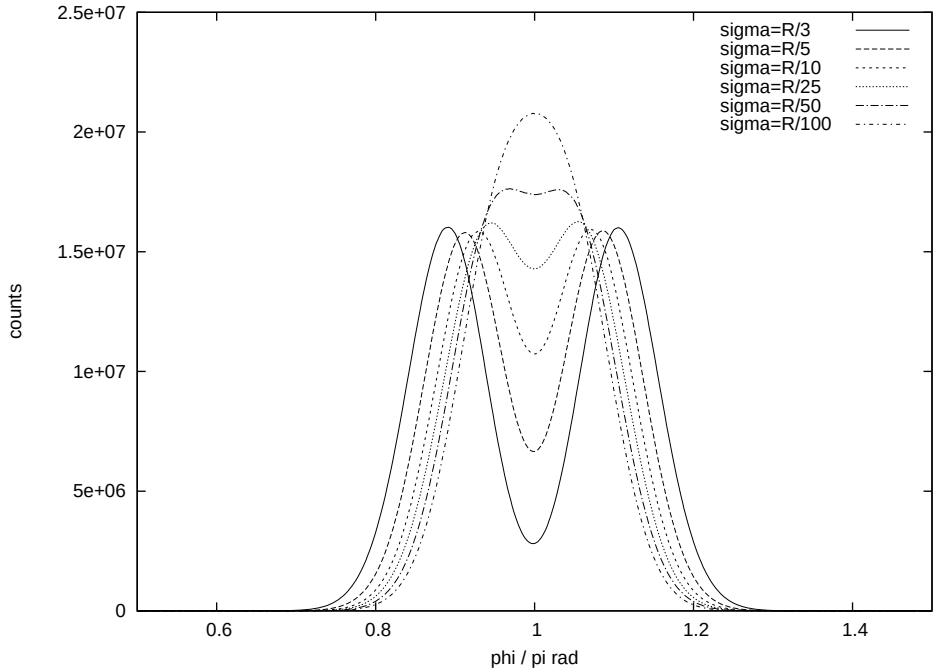

Figure 13: The distribution of two particles for different values of σ. $2 \cdot 10^9$ steps were performed at $T = 0.1nK$.

Although a mapping theorem between fermions and hard core repulsive bosons exists as mentioned above, the distance distributions of the associated cases are still different in their behaviour towards zero distance. In the fermionic case the curve goes directly down to (0/0) whereas in the interacting bosons case distances slightly bigger than zero are extremely suppressed before raising towards the maximum. This is due to the different occupation of momentum states. The bosons still both occupy the lowest states, but at different positions. In contrast to that, the average position of both fermions is still in the minimum of the potential. Since they occupy the first and second state the distribution of the superposition of both particles looks similar to the one of the bosons. But also here are differences in behaviour. So the probability to find the particle in the minimum of the potential would never goes towards zero due to the contribution of the first state having its maximum probability exactly there. On the contrary, when letting σ go towards infinity, the propability in the minimum would go to zero, as one can guess from figure 13.

4.4 Interacting dipoles

The final extension to the code in this projet was the inclusion of a dipole moment for each particle. To describe this system two new coordinates had to be introduced, described in the next section. Furthermore a value for the dipole moment and a moment of inertia, in order to calculate the kinetic part of the density matrix for the new coordinates, had to be chosen. For the dipole one might think of an atom with an excited Rydberg state what can be approximated by $q = 1e$ and $d \simeq 2\text{Å}$. Furthermore we assumed a homogeneous sphere to calculate the moment of inertia. So

$$p = q \cdot d = 1\text{e} \cdot 2\text{Å} = 2\text{e} \cdot 10^{-10} m \tag{53}$$

and

$$J = \frac{2}{5} m r^2 = \frac{2}{5} \cdot 1.419 \cdot 10^{-25}\text{kg} \cdot \left(10^{-10} m\right)^2 \tag{54}$$

4.4.1 Coordinate system

In order to make clear what the following plots actually show, here the used coordinate system is presented. The position of the dipole on the ring is specified by φ. The azimuth of the

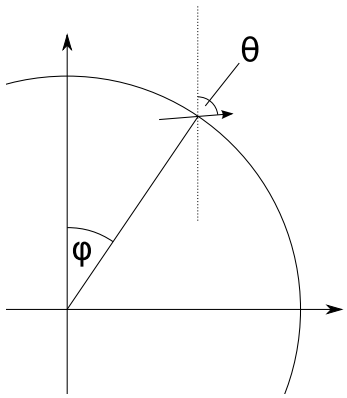

Figure 14: chosen coordinate system

orientation of the dipolemoment is specified by θ with respect to a parallel of the axis to which φ is associated. So for dipoles pointing exactly outwards the ring θ equals φ. The zenith is specified by $\vartheta \in [0; \pi]$. Dipoles pointing upwards exactly perpendicular to the plain in which the ring lies have $\vartheta = 0$.

4.4.2 Dipolar gas ground state

The first thing to observe was how a gas of dipoles minimises its energy. Therefor three dipoles were put into the previous described external potential with its minimum at $\phi = \pi$. In addition to the dipole interaction they are kept apart from each other by the the repulsive potential (52).

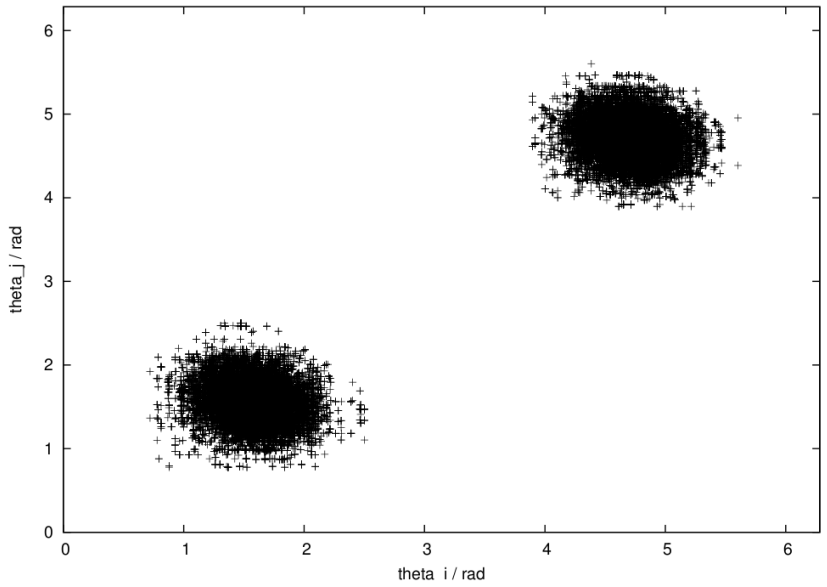

Figure 15: Pair θ-θ correlation for 3 dipoles confined near $\phi = \pi$. Simulated at $T = 0.1nK$

In figure 15 one can see, that the dipoles are always aligned along the ring, since ϕ and θ differ by $\pi/2$. Furthermore the values seem to be strongly correlated, the dipoles always pointing in a similar direction. Together with the next plot (fig. 16), that shows how often a dipole is found with a certain value of θ, we can conclude, that in the ground state of this system either all dipoles pointing clockwise or counterclockwise around the ring and that these two cases are equally common. The different height of the peaks is believed to only be due to the finite number of steps.

When expending this result to a closed circle of dipoles, the basic result would not change, since the periodic boundary condition of the system is somehow implicitly contained in the configuration of the dipoles. They still would point all around the ring in the same direction (with respect to the ring).

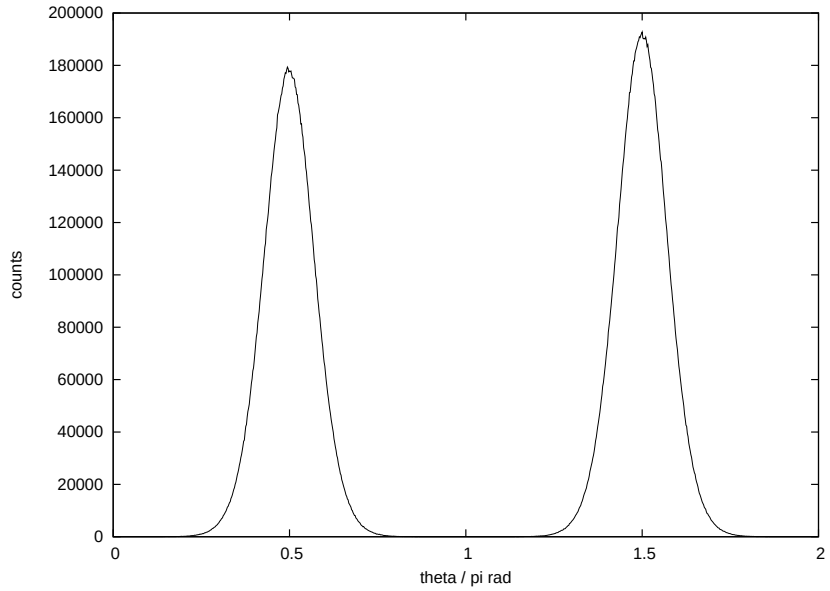

Figure 16: Distribution of θ for 3 dipoles confined near $\phi = \pi$. Simulated within 10^8 steps at $T = 0.1nK$

4.4.3 Spin-like dipoles and frustration

As seen above, dipoles that are not constrained in their movement have a unique ground state when situated on a ring. They all align in the same direction along and around the ring. This creates a closed chain of alternating charge, independent of the number of particles, lowering the energy. The possibility of aligning all in the same way, but the opposite direction is more due to a symmetry of the system then to a degenerated ground state energy.

If one wants to observe interesting features like so called *frustration*, as it can be found in antiferromagnetically or ferrimagnetically coupled spin systems, e.g. spin glasses, one has to restrict the motion of the dipoles. The restriction we introduced is to only allow the dipoles to align in the plane perpendicular to the motion along the ring.

The next figure shows basically the configuration for four particles, if the repulsion is sufficiently high. It is shown to communicate a general feeling for the system's behaviour.

Now for three particles the ground state configuration isn't unique anymore, what is shown in the next picture. One can easily see, that both configurations are energeticly equivalent (due to symmetry in swapping the charge signs) but cannot be mapped on each other by a spatial symmetry and therefore are distinguishable. Our simulations show, that in the statistical average the two configurations shown in figure 18 occur with equal probability. This situation is commonly referred to as *frustration.*

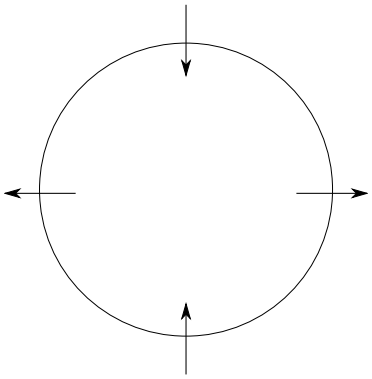

Figure 17: ground state configuration for four dipoles

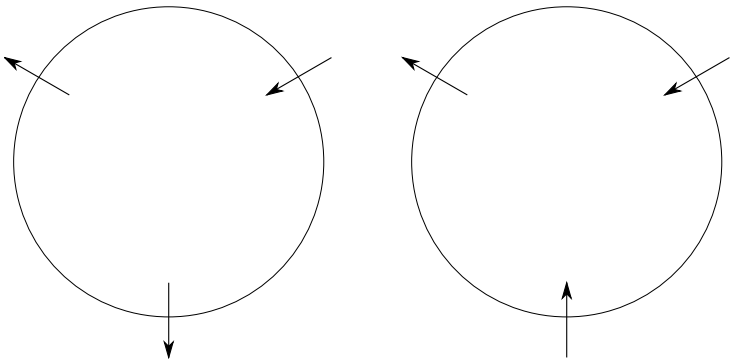

Figure 18: ground state configurations for three dipoles

To investigate the behaviour of this system further, we introduced a new quantity specifying the direction of the dipole. Since the distribution of ϑ has usually a distinct maximum at $\pi/2$ (see figure 19) it is reasonable to generalise to either out pointing or in pointing dipoles. So in figure 18 on the left we would have a $+1$ and on the right a -1 in each case for the dipole at the bottom. So finally to obtain figure 20 we took this quantity and created a correlation to another dipole by multiplying the two values of each of them. So we obtain a $+1$ when they are pointing into the same direction and a -1 when pointing in opposite directions with respect to the ring. This will be referred to as *theta*-correlation. It should be mentioned that this might contain a certain amount of error, since, especially for higher temperatures, there will be configurations, that are recorded as correlated, although actually not correlated. But since the ranges of ϑ, for which such situations are possible, are relatively unlikely, the qualitative information of the following plots is still valid.

Actually plotted is the average of this correlation value against the distance of the two dipoles. Distances with less counts than 1‰ of the maximum in the distance distribution were

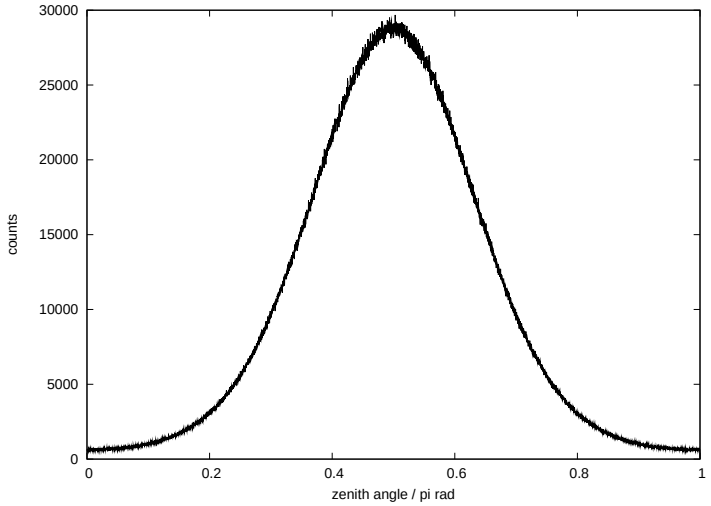

Figure 19: The distribution of ϑ obtained from a 2 particle simulation of 10^8 steps at $T = 0.1nK$.

neglected.

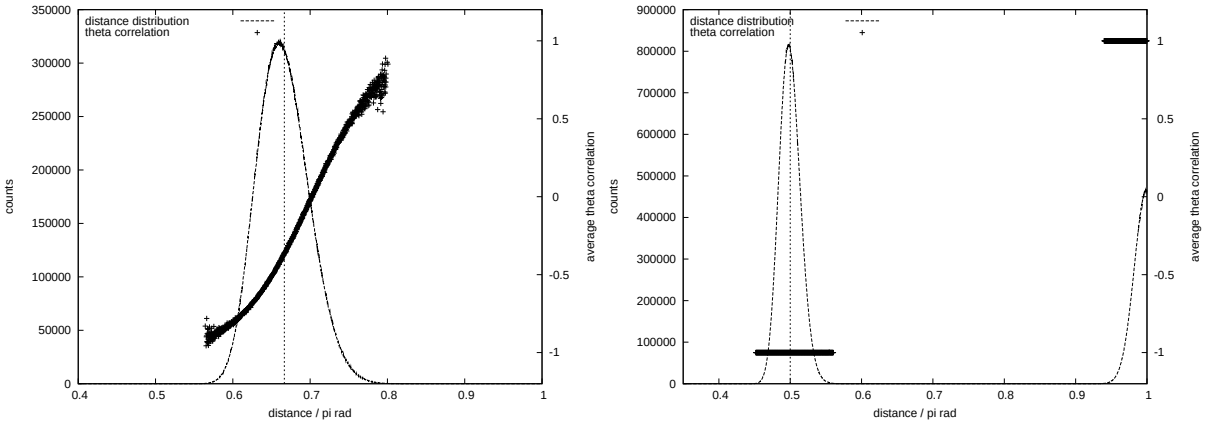

(a) 3 dipoles (b) 4 dipoles

Figure 20: The distance distribution and the average θ correlation for 3 and 4 dipoles, respectively. Simulated with $2 \cdot 10^8$ steps at $T = 0.1nK$. The gap for four dipoles is due to neglecting distances with less counts than 1‰ of the maximum.

The most obvious matter in these two plots is the difference in the θ-correlation between an even and an odd number of particles (for five and six particles the two plots would qualitatively be the same). For four particles there are two clearly separated regions with distinct correlation. The dipoles are commonly $\pi/2$ apart from each other and show an alternating correlation, what exactly was shown in figure 17.

For three particles the situation is a bit more complex. First of all one can recognise an asymmetry in the distance distribution, the right hand side decays slower than the left hand side. This is probably due to the different dependences towards the distance of the two parts of the potential. The dipole interaction goes basically with $1/d^3$, whereas the repulsion goes with $1/d^{12}$, so the total potential is not the same at the two sides. One might argue, that the third particle would restor the symmetry, but since we are plotting a pair distance distribution, the distance to the third particle is averaged here, so the asymmetry persists. What one would expect for the θ-correlation is to find it be zero, since both configurations are equally common. Indeed there is a certain distance where the value is zero, but when moving to either side it goes to 1 and -1, respectively. In these configurations the distance to one of the other two dipoles is smaller and so it is energetically favourable to align antiparallel to the dipole that is closer. We think this form of the graph is a good signature of a frustrated (spin-like) system. Surprisingly the correlation is not zero at the maximum of the distance distribution near $2\pi/3$, indicated by the dashed line. This might be due to the above mentioned asymmetry but needs further investigation to be clarified.

In the following the dependence or stability of the above described correlation and frustration, respectively, will be investigated. The first point is the behaviour of the alternating correlation at higher temperatures. In figure 21 the red lines are the same as in figure 20 for four particles.

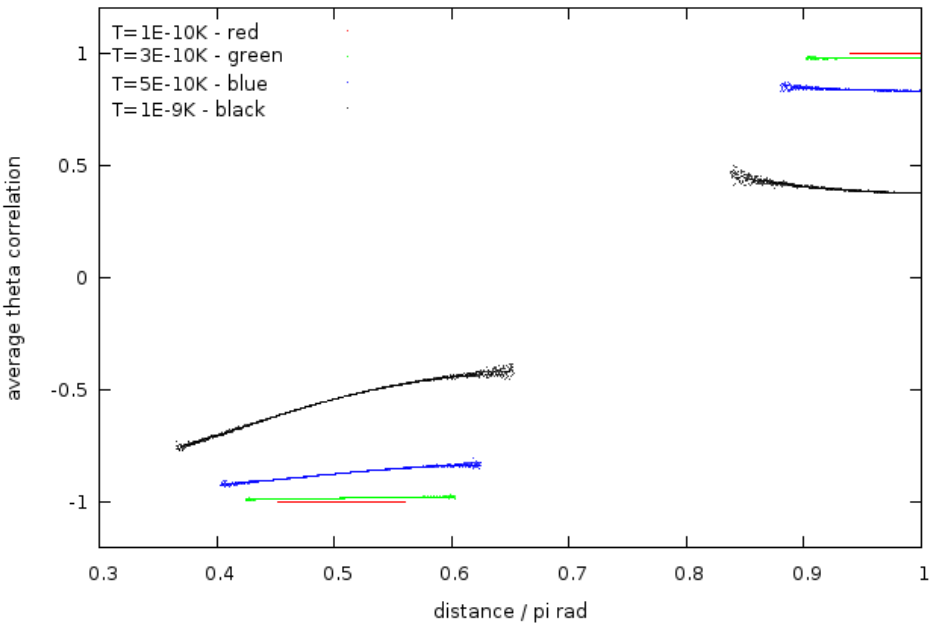

Figure 21: The average θ correlation for 4 dipoles simulated at different temperatures with $4 \cdot 10^9$ steps.

With increasing temperature the correlation becomes weaker and also starts to show a distance dependency, similar to the one observed for three particles. This is due to the stronger interaction at shorter distances, so the thermal fluctuations can be compensated better. It is surprising, that already for still very low temperatures like $10^{-9}K$ the correlation starts to vanish.

We saw, that the frustration started to disappear if the particles aren't equally distributed, so they have to be kept apart from each other. To point out this important condition, we again plotted figure 20 for three particles, but with a potential one order of magnitude weaker.

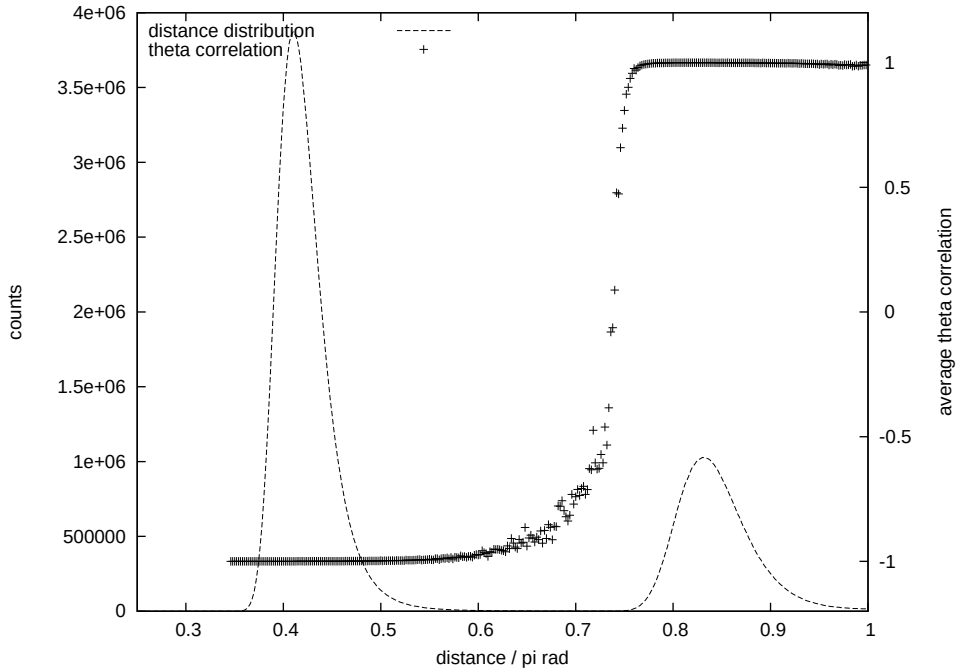

Figure 22: The distance distribution and the average θ correlation for 3 dipoles in a, in comparison with the above plots, weak potential. Simulated with 10^8 steps at $T = 0.1nK$.

The distance distribution shows, that now all three particles can be found within π, i.e. are situated on one half of the ring. The frustration signature doesn't occur anymore, but a distinct alternating correlation for the most probable regions. Only in the very unlikely intermediate region one can observe a steep but smooth transition from -1 to 1.

Furthermore we were interested whether the observed configuration is conserved for higher number of particles or a correlation length for the θ-correlation can be found. Therefor different numbers of particles were simulated while maintaining the density (by increasing the size of the ring) and the repulsive interaction (The problem occurred, that although the distance between the particles is the same, even the existence of more particles, all contributing to the total potential a particle experiences, the confinement increased rapidly). In order to compensate

this effect σ was reduced for higher numbers of particles. The plot (fig. 23) shows a decrease

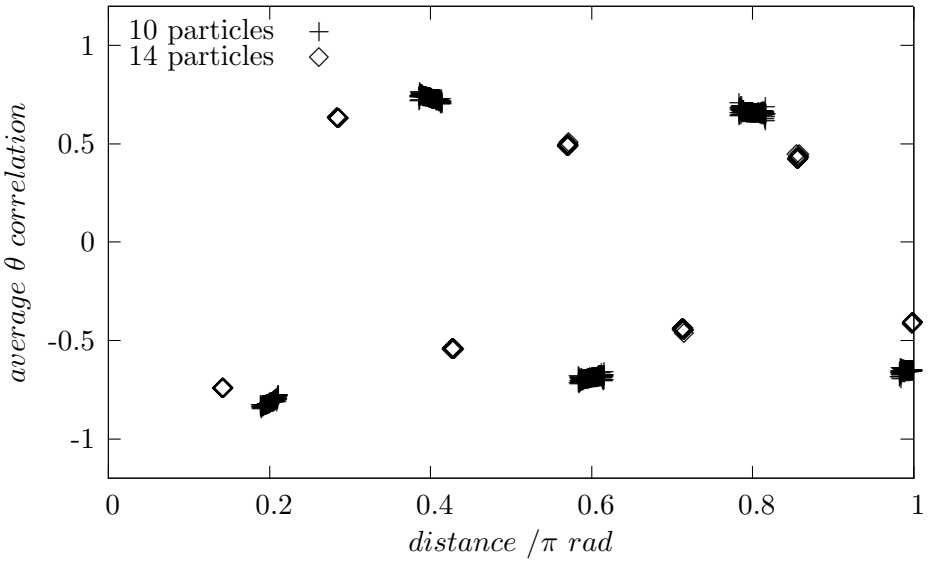

Figure 23: The average θ correlation for 10 and 14 dipoles, respectively, simulated providing a constant density and nearly constant repulsive potential with $4 \cdot 10^8$ steps at $T = 0.1nK$.

of correlation with increasing particle number as well as a decrease with larger distance. The decrease due to the particle number, observed at the shortest distance, is quite weak and occurs probably because of the noise the other dipoles produce. The decay for larger distances is stronger. It seems, the more dipoles their are in between a pair communicating between them, the weaker is the correlation between this pair. In which way this decay takes place and what the the typical correlation length is could be investigated in further research.

5 Conclusions

5.1 Summary

In this project a PIQMC code was realised capable to simulate various systems from a single particle on a one dimensional ring to n interacting dipoles on such a ring. It was possible to verify its operativeness in terms of comparison of ground state energies for single particles as well as for (anti-)symmetrised many particle systems. Different interactions were implemented and, although not analytical verifiable, show trustable effects, consistent with physical theory. Significant signs of Bose-Einstein condensation couldn't be obtained, but we were able to reproduce the signatures of a Tonks-Girardeau gas. It was shown that *frustration* can be obtained

using a closed chain of dipoles when restricting their motions. Finally some properties of this dipole chain were observed.

5.2 Experimental realisation

As presented in this report, it is theoretically possible to obtain frustrated systems in rings of atomic dipoles. However, an experimental realisation might be extremely challenging or even impossible. In addition to the fact, that the restriction in motion of the dipoles have to be realised in a way, there are a number of other difficulties. The most serious one is the condition of extremely low temperatures of $0.1nK$. Recent experiments can reach $10nK$. Furthermore it was observed, that repulsion between the particles has to be sufficiently strong to stay in the frustrated regime. The last point to mention is the effect of increasing particle number, making the system noisier. Therefore it probably will be more difficult to obtain a clear signature of frustration.

5.3 Further Research

Further effort should be made particularly in increasing the number of particles that can be simulated. This basically means increasing the efficiency of obtaining the symmetrisation, but also make the sampling more efficient to reduce the number of necessary Monte Carlo steps. An approach to the first point might be to sample through permutations in a Monte Carlo like way rather than calculating the exact permanent for each step [8]. The latter one could be realised by implementing path shifting and bi-sectional sampling.

Provided with these improvements the observation of a Bose-Einstein condensate and the determination of properties of many dipole chains might be possible.

6 Acknowledgement

First and foremost I want to thank my supervisor Ian Galbraith and his PhD student Peter McDonald. Our discussions were always helpfull and pushed the whole project continuously forward.

Furthermore a thanks goes to Patrick Öhberg who often assisted in questions of atomic physics.

7 Appendices

A Dipole interaction

The potential of a dipole is known to be

$$\phi^{dipole}(\vec{r}) = \frac{1}{4\pi\varepsilon}\frac{\vec{r}\cdot\vec{p}}{r^3} \tag{55}$$

if the distance $|\vec{r}|$ is much larger than the size of the dipole. The interaction energy of a dipole in an external field is

$$V^{dipole} = -\vec{p}\cdot\vec{E} = \vec{p}\cdot grad\ \phi^{dipole}(\vec{r}) \tag{56}$$

Substituting the potential into this yields

$$\begin{aligned} V^{dipole} &= \vec{p}_2 \cdot grad\frac{1}{4\pi\varepsilon}\frac{\vec{r}\cdot\vec{p}_1}{r^3} \\ &= \vec{p}_2 \cdot \left(\frac{1}{4\pi\varepsilon r^3}\left(\vec{p}_1 - 3\frac{(\vec{r}\cdot\vec{p}_1)\vec{r}}{r^2}\right)\right) \\ &= \frac{1}{4\pi\varepsilon r^3}\left(\vec{p}_2\cdot\vec{p}_1 - 3\frac{(\vec{r}\cdot\vec{p}_1)(\vec{r}\cdot\vec{p}_2)}{r^2}\right) \end{aligned} \tag{57}$$

Using the coordinates described in 4.4.1 we can express the variables as

$$\vec{r} = \vec{r}_2 - \vec{r}_1 = R\begin{pmatrix}\cos\varphi_2 - \cos\varphi_1\\ \sin\varphi_2 - \sin\varphi_1\\ 0\end{pmatrix} \quad \vec{p}_1 = p\begin{pmatrix}\cos\theta_1\sin\vartheta_1\\ \sin\theta_1\sin\vartheta_1\\ \cos\vartheta_1\end{pmatrix} \quad \vec{p}_2 = p\begin{pmatrix}\cos\theta_2\sin\vartheta_2\\ \sin\theta_2\sin\vartheta_2\\ \cos\vartheta_2\end{pmatrix} \tag{58}$$

Substituting this into (57) and simplifying using *Mathematica* gives

$$V^{dipole} = \frac{p^2}{4\pi\varepsilon r^3}\left(\cos\vartheta_1\cos\vartheta_2 - 0.5[\cos(\theta_1-\theta_2) - 3\cos(\theta_1-\theta_2-\varphi_1-\varphi_2)]\sin\vartheta_1\sin\vartheta_2\right) \tag{59}$$

So for n dipoles one gets

$$V^{dipole}_{total} = \frac{p^2}{8\pi\varepsilon}\sum_{i}^{n}\sum_{j\neq i}^{n}\frac{1}{r^3_{ij}}\left(\cos\vartheta_i\cos\vartheta_j - 0.5[\cos(\theta_i-\theta_j) - 3\cos(\theta_i-\theta_j-\varphi_i-\varphi_j)]\sin\vartheta_i\sin\vartheta_j\right) \tag{60}$$

B Virial calculations

In this part we will employ the Virial theorem (48) to obtain the kinetic energies associated with the implemented potentials.

B.1 External potential

The external potential used for certain simulations was chosen to be

$$V^{ext} = V_0^{ext} \cdot (1 + \cos\varphi) \tag{61}$$

Employing the Virial theorem gives the kinetic energy to be

$$T^{ext} = \frac{1}{2}\varphi \cdot \frac{\partial V^{ext}}{\partial \varphi} = -\frac{V_0^{ext}}{2}\varphi \cdot \sin\varphi \tag{62}$$

It turned out that this expression doesn't give the correct result. This is due to the potential has his symmetry at $\varphi = \pi$ rather than $\varphi = 0$. So the expression that can be found in the code is

$$T^{ext} = -\frac{V_0^{ext}}{2}(\varphi - \pi) \cdot \sin\varphi \tag{63}$$

where the distance was shifted with respect to the minimum.

B.2 Lennard-Jones potential

The repulsive part of the total potential was chosen to be Lennard-Jones like, where only the repulsive part is used.

$$V^{LJ} = \frac{1}{2}V_0^{LJ}\sum_{i}^{n}\sum_{j\neq i}^{n}\left(\frac{\sigma}{d_{ij}}\right)^{12} \tag{64}$$

Here we used $d_{ij} = |\vec{r}_i - \vec{r}_j|$. It is clear that $\frac{\partial d_{ij}}{\partial \vec{r}_i} = -\frac{\partial d_{ij}}{\partial \vec{r}_j}$ and so we can modify the virial formula as follows

$$\vec{r}_i \cdot \frac{\partial V^{LJ}}{\partial \vec{r}_i} + \vec{r}_j \cdot \frac{\partial V^{LJ}}{\partial \vec{r}_j} = (\vec{r}_i - \vec{r}_j) \cdot \frac{\partial d_{ij}}{\partial \vec{r}_i} \cdot \frac{\partial V^{LJ}}{\partial d_{ij}} = d_{ij} \cdot \frac{\partial V^{LJ}}{\partial d_{ij}} \tag{65}$$

Using this result we get

$$\begin{aligned} T^{LJ} &= -\frac{1}{4}V_0^{LJ}\sum_i^n\sum_{j\neq i}^n d_{ij}\cdot\frac{\partial}{\partial d_{ij}}\left(\frac{\sigma}{d_{ij}}\right)^{12} \\ &= \frac{1}{4}V_0^{LJ}\sum_i^n\sum_{j\neq i}^n 12\cdot d_{ij}\cdot\frac{\sigma^{12}}{d_{ij}^{13}} \\ &= 6\cdot\left[\frac{1}{2}V_0^{LJ}\sum_i^n\sum_{j\neq i}^n\left(\frac{\sigma}{d_{ij}}\right)^{12}\right] \\ T^{LJ} &= 6\cdot V^{LJ} \end{aligned} \tag{66}$$

B.3 Dipole interaction

In the last part the virial of the dipole interaction, derived in appendix A, will be deduced.

The vector $\vec{r}$ in (48) can now be identified with $\vec{r}=(\varphi,\theta,\vartheta)$. Therefore we can obtain the kinetic energy of the dipole interaction, using (59), by calculating

$$\begin{aligned} T^{dipole} = \frac{1}{2}\sum_i^n\sum_{j\neq i}^n\frac{1}{2}\Bigg(&\varphi_i\cdot\frac{\partial V_{ij}^{dipole}}{\partial\varphi_i}+\varphi_j\cdot\frac{\partial V_{ij}^{dipole}}{\partial\varphi_j}+\theta_i\cdot\frac{\partial V_{ij}^{dipole}}{\partial\theta_i} \\ &+\theta_j\cdot\frac{\partial V_{ij}^{dipole}}{\partial\theta_j}+\vartheta_i\cdot\frac{\partial V_{ij}^{dipole}}{\partial\vartheta_i}+\vartheta_j\cdot\frac{\partial V_{ij}^{dipole}}{\partial\vartheta_j}\Bigg) \end{aligned} \tag{67}$$

This was again done by *Mathematica* giving

$$\begin{aligned} T^{dipole} = \sum_i^n\sum_{j\neq i}^n\frac{p^2}{R^3\sin^3\left(\frac{\varphi_i-\varphi_j}{2}\right)}\Bigg\{&\cos(\vartheta_i)\Bigg(-0.09375\cdot\varphi_i\cdot\cos(\vartheta_j)\cot\left(\frac{\varphi_i-\varphi_j}{2}\right) \\ &+\vartheta_i\Big[-0.03125\cos(\theta_i-\theta_j)+0.09375\cos(\theta_i+\theta_j-\varphi_i-\varphi_j)\Big]\sin(\vartheta_j)\Bigg) \\ &+\sin(\vartheta_i)\Bigg(-0.0625\cdot\vartheta_i\cdot\cos(\vartheta_j)+\Big[\varphi_i\big\{0.046875\cos(\theta_1-\theta_2) \\ &-0.140625\cos(\theta_i+\theta_j-\varphi_i-\varphi_j)\big\}\cot\left(\frac{\varphi_i-\varphi_j}{2}\right)+0.03125\cdot\theta_i\cdot\sin(\theta_i-\theta_j) \\ &+0.09375(\varphi_1-\theta_1)\sin(\theta_i+\theta_j-\varphi_i-\varphi_j)\Big]\sin(\vartheta_j)\Bigg)\Bigg\} \end{aligned} \tag{68}$$

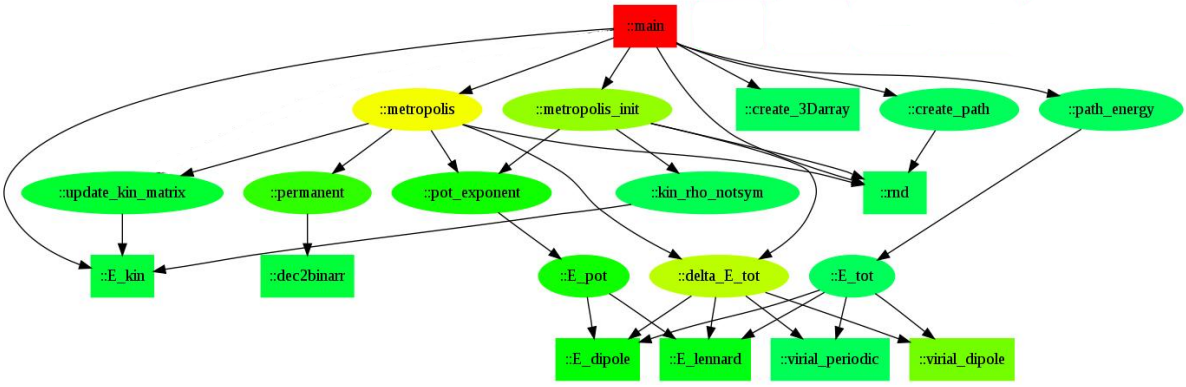

Figure 24: full code structure

C Program structure

The three functions in the upper right corner perform the creation and evaluation of the path. A three dimensional array is created for storing the path. With the next function the actual path is created. Since this function points on the *rnd* function, the random number generator function is employed. The third function of this group calculates the total energy of the initial path, employing all potential and virial functions.

The function *metropolis_init* employs the function *kin_rho_notsym* and doesn't use symmetrisation, whereas *metropolis* employs *permanent* and so includes symmetrisation. *Update_kin_matrix* recalculates the values of the array *kin_matrix* after a trial move. The function *delta_E_tot* calculates the energy change caused by the trial move.

References

[1] A. Arkhipov, G. Astrakharchik, A. Belikov, and Y. Lozovik. Ground-state properties of a one-dimensional system of dipoles. *JETP LETTERS*, 82(1):39–43, 2005.

[2] G. E. Astrakharchik and Y. E. Lozovik. Super-Tonks-Girardeau regime in trapped one-dimensional dipolar gases. *PHYSICAL REVIEW A*, 77(1), JAN 2008.

[3] G. E. Astrakharchik, G. Morigi, G. De Chiara, and J. Boronat. Ground state of low-dimensional dipolar gases: Linear and zigzag chains. *PHYSICAL REVIEW A*, 78(6, Part B), DEC 2008.

[4] D. Ceperly. Path integrals in the theory of condensed helium. *Rev. Mod. Phys.*, 67(2):279–355, APR 1995.

[5] R. P. Feynman. Space-time approach to non-relativistic quantum mechanics. *Rev. Mod. Phys.*, 20(2):367–387, Apr 1948.

[6] R. P. Feynman. Space-time approach to quantum electrodynamics. *Phys. Rev.*, 76(6):769–789, Sep 1949.

[7] R. P. Feynman. The λ-transition in liquid helium. *Phys. Rev.*, 90(6):1116–1117, Jun 1953.

[8] S. Franke-Arnold, J. Leach, M. J. Padgett, V. E. Lembessis, D. Ellinas, A. J. Wright, J. M. Girkin, P. Ohberg, and A. S. Arnold. Optical ferris wheel for ultracold atoms. *OPTICS EXPRESS*, 15(14):8619–8625, JUL 9 2007.

[9] H. Hinrichsen. Computational physics - lecture script.

[10] G. M. Relationship between systems of impenetrable bosons and fermions in one dimension. *J. Math. Phys.*, 1(6):516–523, 1960.

[11] R. MacKenzie. Path integral methods and applications, 2000.

[12] B. Paredes, A. Widera, V. Murg, O. Mandel, S. Folling, I. Cirac, G. Shlyapnikov, T. Hansch, and I. Bloch. Tonks-Girardeau gas of ultracold atoms in an optical lattice. *NATURE*, 429(6989):277–281, MAY 20 2004.

[13] H. J. Ryser. *Combinatorical Mathematics*, volume 14 of *Carus Mathematical Monographs*. The Mathematical Association of America, 1963.

[14] G. Toulouse. Theory of the frustration effect in spin glasses. i. *Communications on Physics*, 2(4):115–119, 1977.

[15] G. H. Wannier. Antiferromagnetism. the triangular ising net. *Phys. Rev.*, 79(2):357–364, Jul 1950.